This article was downloaded by: [154.6.24.240] On: 29 May 2022, At: 12:17
Publisher: Institute for Operations Research and the Management Sciences (INFORMS)
INFORMS is located in Maryland, USA

Transportation Science

Publication details, including instructions for authors and subscription information:
http://pubsonline.informs.org

Equilibrium Analysis of Urban Traffic Networks with Ride-Sourcing Services

https://orcid.org/0000-0001-5626-285XZhengtian Xu, Zhibin Chen, Yafeng Yin, https://orcid.org/0000-0001-8662-5818Jieping Ye

To cite this article:
https://orcid.org/0000-0001-5626-285XZhengtian Xu, Zhibin Chen, Yafeng Yin, https://orcid.org/0000-0001-8662-5818Jieping Ye (2021) Equilibrium Analysis of Urban Traffic Networks with Ride-Sourcing Services. Transportation Science 55(6):1260-1279. https://doi.org/10.1287/trsc.2021.1078

Full terms and conditions of use: https://pubsonline.informs.org/Publications/Librarians-Portal/PubsOnLine-Terms-and-Conditions

This article may be used only for the purposes of research, teaching, and/or private study. Commercial use or systematic downloading (by robots or other automatic processes) is prohibited without explicit Publisher approval, unless otherwise noted. For more information, contact permissions@informs.org.

The Publisher does not warrant or guarantee the article's accuracy, completeness, merchantability, fitness for a particular purpose, or non-infringement. Descriptions of, or references to, products or publications, or inclusion of an advertisement in this article, neither constitutes nor implies a guarantee, endorsement, or support of claims made of that product, publication, or service.

Copyright © 2021, INFORMS

Please scroll down for article—it is on subsequent pages

With 12,500 members from nearly 90 countries, INFORMS is the largest international association of operations research (O.R.) and analytics professionals and students. INFORMS provides unique networking and learning opportunities for individual professionals, and organizations of all types and sizes, to better understand and use O.R. and analytics tools and methods to transform strategic visions and achieve better outcomes.
For more information on INFORMS, its publications, membership, or meetings visit http://www.informs.org

http://pubsonline.informs.org/journal/trsc

TRANSPORTATION SCIENCE
Vol. 55, No. 6, November–December 2021, pp. 1260–1279
ISSN 0041-1655 (print), ISSN 1526-5447 (online)

Equilibrium Analysis of Urban Traffic Networks with Ride-Sourcing Services

Zhengtian Xu,[a] Zhibin Chen,[b] Yafeng Yin,[c,*] Jieping Ye[d]

[a] Department of Civil and Environmental Engineering, The George Washington University, Washington, District of Columbia 20052; [b] Division of Engineering and Computer Science, New York University Shanghai, Shanghai 200122, China; [c] Department of Civil and Environmental Engineering, University of Michigan, Ann Arbor, Michigan 48109; [d] DiDi AI Labs, Didi Chuxing, Beijing 100085, China
*Corresponding author

Contact: zhengtian@gwu.edu, https://orcid.org/0000-0001-5626-285X (ZX); chipin@umich.edu, https://orcid.org/0000-0002-5425-6189 (ZC); yafeng@umich.edu, https://orcid.org/0000-0003-3117-5463 (YY); yejieping@didichuxing.com, https://orcid.org/0000-0001-8662-5818 (JY)

Received: July 18, 2019
Revised: June 30, 2020; December 27, 2020; May 24, 2021
Accepted: May 27, 2021
Published Online in Articles in Advance: October 19, 2021

https://doi.org/10.1287/trsc.2021.1078

Copyright: © 2021 INFORMS

Abstract. Ride-sourcing services play an increasingly important role in meeting mobility needs in many metropolitan areas. Yet, aside from delivering passengers from their origins to destinations, ride-sourcing vehicles generate a significant number of vacant trips from the end of one customer delivery trip to the start of the next. These vacant trips create additional traffic demand and may worsen traffic conditions in urban networks. Capturing the congestion effect of these vacant trips poses a great challenge to the modeling practice of transportation planning agencies. With ride-sourcing services, vehicular trips are the outcome of the interactions between service providers and passengers, a missing ingredient in the current traffic assignment methodology. In this paper, we enhance the methodology by explicitly modeling those vacant trips, which include cruising for customers and deadheading for picking up them. Because of the similarity between taxi and ride-sourcing services, we first extend previous taxi network models to construct a base model, which assumes intranode matching between customers and idle ride-sourcing vehicles and thus, only considers cruising vacant trips. Considering spatial matching among multiple zones commonly practiced by ride-sourcing platforms, we further enhance the base model by encapsulating internode matching and considering both the cruising and deadheading vacant trips. A large set of empirical data from Didi Chuxing is applied to validate the proposed enhancement for internode matching. The extended model describes the equilibrium state that results from the interactions between background regular traffic and occupied, idle, and deadheading ride-sourcing vehicles. A solution algorithm is further proposed to solve the enhanced model effectively. Numerical examples are presented to demonstrate the model and solution algorithm. Although this study focuses on ride-sourcing services, the proposed modeling framework can be adapted to model other types of shared use mobility services.

Funding: The work described in this paper was partly supported by the National Science Foundation [Grants CMMI-1740865, CMMI-1854684, and CMMI-1904575], the Center for Connected and Automated Transportation at the University of Michigan, and Didi Chuxing.
Supplemental Material: The online appendix is available at https://doi.org/10.1287/trsc.2021.1078.

Keywords: ride-sourcing systems • vacant trips • network equilibrium • traffic congestion

1. Introduction

Recent advancements in information and vehicular technologies are driving an unprecedented wave of innovations in mobility services. Specifically, the number of smart mobile devices in the United States has been rising steadily, and studies suggest that over 80% of Americans now own at least one such device (Anderson 2019). These devices retrieve users' geolocations, enable ubiquitous communications, and allow instant peer-to-peer interaction, giving rise to various on-demand mobility services that connect suppliers of resources and services to their customers with very low transaction costs (Greer et al. 2018). As a typical example of emerging mobility services, ride sourcing and ride-sourcing companies (also known as transportation network companies) have attracted much attention and achieved substantial growth in recent years. In particular, Uber has cumulatively served over 10 billion customer trips and extended its business to 65 countries on six continents, whereas Didi Chuxing provides 30 million daily rides and has covered more than 400 cities globally as of May 2019 (Iqbal 2019). These ride-sourcing services are expected to play an increasingly important role in meeting mobility needs. It is therefore critical to better understand their implications on the system performance of urban traffic networks.

Recent evidence shows that the expansion of ride-sourcing markets has already contributed substantially to the deteriorating traffic conditions in some major cities (Castiglione et al. 2018; Schaller 2018; Erhardt et al. 2019). Ride-sourcing customers are those who give up their own vehicles or switch from traditional taxi, public transportation, or other nonmotorized modes. In serving these customers, ride-sourcing vehicles (RVs) generate massive vacant trips. These vacant trips create additional traffic demand and worsen traffic conditions. Although transportation planning agencies have shown great interest in the congestion impact estimates of ride-sourcing services, developing the right methodology to do so presents a great challenge. This paper aims to tackle this challenge.

Conventional trip-based travel demand forecasting models forecast the future-year traffic flow of a traffic network using a four-step process: (i) trip generation, where the total production and attraction of trips from/to each zone are quantified; (ii) trip distribution, where a destination choice model is used to generate the demand for travel between any two given zones in the network; (iii) mode choice, where the number of person-trips using personal vehicles for travel is identified and converted to vehicular trips based on fixed vehicle-occupancy factors; and (iv) traffic assignment, where user equilibrium assignment models are used to assign vehicular trips to the network, ensuring that no vehicle would be better off by unilaterally changing its route. With ride-sourcing services, vehicular trips are the outcome of the interactions between service operators and passengers and can no longer be easily determined by applying fixed vehicle-occupancy factors. More specifically, to serve a given passenger demand pattern, the corresponding occupied vehicular trip pattern can be determined similarly as before. Nonetheless, the associated vacant vehicular trips, which result from vacant RVs' behaviors of searching for passengers (hereinafter referred to as cruising trips) and picking up passengers (called deadheading trips by Ban et al. 2019), are beyond the reach of traditional analyses. We note that a substantial portion of vacant or empty vehicle miles traveled (VMTs) in the system is a common feature shared by other shared mobility service systems. It thus becomes increasingly important for transportation planners to model these vacant trips in their modeling practices. We further note that the state-of-the-art activity-based models also suffer the same limitation as their trip-based predecessors. Therefore, there is a pressing need to enhance existing traffic assignment models to adequately account for vacant trips in shared mobility systems. Representing one of the early efforts in this objective, this paper develops a static user equilibrium assignment model to capture the network congestion effects of ride-sourcing services.

Ride sourcing shares similarities with traditional taxi services (Zha, Yin, and Yang 2016). A large body of literature has been devoted to network equilibrium analyses of taxi markets. Yang and Wong (1998) made the first attempt to mathematically model the movements of both vacant and occupied taxis in a network context and investigated the equilibrium state of taxi services. It is assumed that after an occupied taxi becomes vacant, it will select a target zone to seek out customers based on a logit model aiming to minimize its expected vacant time. After picking up a customer, the taxi will choose a predetermined shortest route to finish the trip. Their model was then extended by considering the market competition and regulation (Yang, Wong, and Wong 2002), bilateral taxi-customer searching and meeting (Yang et al. 2010), and multiple types of taxis (i.e., street hailing and e-hailing) (He and Shen 2015). Despite the abundant literature in modeling taxi services, only a few studies have considered congestion because of the routing behaviors of both vacant and occupied taxis. Specifically, Wong, Wong, and Yang (2001) extended the model by Yang and Wong (1998) to further incorporate congestion effects as well as the customer demand elasticity. A bilevel framework was proposed to describe the stationary state of taxi movements. At the lower level, given the customer generation and attraction of each zone, a convex mathematical problem delineates the movements of both vacant and occupied taxis in congested road networks. At the upper level, a set of equations describes the relationships among waiting times of taxi and customer, the taxi supply, and the customer demand. Recently, Wong et al. (2008) further extended the model to consider multiple user classes and vehicle modes (e.g., luxury taxis and normal taxis). All these prior studies have laid a solid foundation for our work. As intended, they are applicable to modeling street-hailing taxi systems where matching and meeting occur simultaneously, and thus, deadheading trips do not exist. In other words, these models consider cruising trips, which only constitute a portion of vacant trips generated by RVs. To facilitate the presentation of the core idea of this paper, we view street hailing as a form of intranode matching between customers and vacant vehicles, in which customers can only be matched to vacant vehicles at the same node and thus, deadheading is negligible.

More recently, Ban et al. (2019) proposed a traffic assignment model for transportation systems with ride-sourcing services and flow congestion. It is different from the previous models (e.g., Wong, Wong, and Yang 2001; Wong et al. 2008) in that vacant RVs are assumed to follow the dispatch from a centralized control platform that attempts to maximize the total profit. This assumption can simplify the matching and meeting process between customers and vacant RVs. Consequently, the proposed model only considers deadheading trips while ignoring the cruising portion of vacant VMTs. In practice, after dropping off a

customer and before being matched with the next one, idle RVs decide where to go to search for customers. Instead of being dispatched by a control center, idle RVs determine their cruising for customer strategies based on their individual interests.

In existing ride-sourcing systems, cruising and deadheading portions occupy approximately one-third and one-sixth of an RV's effective working hours in major metropolises, respectively. To better account for vacant vehicular miles, this paper develops, to our best knowledge, the first network equilibrium model that considers both the cruising and deadheading trips generated by RVs. In developing the model, we attempt to strike the right balance between the model realism and mathematical tractability. To this aim, we first extend the modeling framework of Yang and Wong (1998) to describe the network equilibrium state that results from the interactions among occupied and idle RVs as well as the background regular traffic. The network equilibrium model considers intranode matching between customers and idle RVs and thus, only captures the congestion impacts of cruising trips. We then consider the internode matching between customers and idle RVs, which appears to be a common practice in ride-sourcing markets (see Section 3.3 for empirical evidence). Because of the spatial heterogeneity in the ride-sourcing market, e-hailing platforms often match idle RVs from zones with excessive vehicle supply to those experiencing a shortage, which yields a substantial number of deadheading VMTs (referred to as "wild goose chase" in Castillo, Knoepfle, and Weyl (2016) and further investigated by Zha, Yin, and Xu (2018) and Xu, Yin, and Ye (2020)). Our extended model describes the outcome of internode matching and captures the congestion effects of both the cruising and deadheading trips generated by RVs.

The remainder of this paper is organized as follows. Section 2 introduces the network equilibrium model with the intranode matching assumption, which serves as our base model. Section 3 proposes an enhanced model to recapitulate the internode matching between drivers and riders and then, validates it using the empirical data from Didi Chuxing. Section 4 extends the base model by replacing the intranode matching with the internode matching counterparts. A solution algorithm is developed for the extended model, which is implemented to solve numerical examples in Section 5. Comparative analyses are subsequently conducted and interpreted. Lastly, Section 6 concludes the paper and points out future research directions.

2. Base Model

Consider a road network $G(V, A)$, where V is the set of nodes and A is the set of links in the network. Each node denotes a traffic analysis zone where travel demand is generated from or attracted to or a change in road geometry/characteristics, whereas each link represents a road segment connecting two neighboring nodes. For the base model, we assume that the matching radius adopted by the e-hailing platform is relatively small such that customers who request rides from the platform will only be matched to idle RVs nearby (mathematically, at the same node). Consequently, deadheading to pick up customers is negligible. The major components of the base model are described in the rest of the section. A complete notational glossary is provided in Table 1 for reference.

2.1. Customer Demand

Denote the node sets R, S as the origins and destinations, respectively, of customer demands, and let W be the set of origin-destination (OD) pairs. Define β^o and β^i as the out-of-vehicle and in-vehicle value of time ($/h), respectively. Then, the travel cost C_{rs} between OD pair $(r,s) \in W$ is given by

$$C_{rs} = F_{rs} + \beta^o w_r^c + \beta^i h_{rs}, \ \forall\ (r,s) \in W,$$

where h_{rs} is the equilibrium or shortest vehicular travel time between node r and s. The trip fare F_{rs} between the nodes is assumed to follow the structure of $F_{rs} = F_{rs}^0 + \beta^f h_{rs}$, where $\beta^f h_{rs}$ represents the time-based component with $\beta^f (\geq 0)$ characterizing the hourly surcharge and F_{rs}^0 denotes a constant for the other time-irrelevant components. w_r^c is the customer's average waiting time at node r.

Assuming the customer demand Q_{rs} to be a strictly decreasing and convex function of the trip cost C_{rs}, we then have

$$Q_{rs} = f_{rs}\left(\beta^o w_r^c + (\beta^i + \beta^f) h_{rs}\right), \ \forall\ (r,s) \in W, \qquad (1)$$

where $f_{rs}' < 0$ and $f_{rs}'' \geqslant 0$. Moreover, assume $\lim_{w_r^c \to +\infty} w_r^c \cdot f_{rs}(w_r^c | \boldsymbol{h}) \in (0, +\infty)$, implying that there are always finite (small) numbers of customers waiting on each origin node no matter how long they wait.

2.2. Idle RV Supply

The idle RVs refer to the group of ride-sourcing vehicles that are vacant waiting to be matched. Typically, idle RVs emerge at destination node set S where they drop off customers and disappear at origin node set R where they get matched to new riders. In this paper, we assume that, after dropping off a passenger, idle RVs will select and then cruise to a target zone to "search" for customers. Suppose the utility function of an idle RV cruising from node $s \in S$ to node $r \in R$ is prescribed as

$$U_{sr} = \bar{F}_r - \gamma \cdot (\bar{h}_r + h_{sr} + w_r^v), \ \forall\ s \in S, r \in R, \qquad (2)$$

where $\bar{F}_r$ and $\bar{h}_r$ are the average fare and service time of the customer trips originating from node r. w_r^v is the idle RV's average waiting time for matching or meeting at node r, and γ denotes ride-sourcing drivers' value of time ($/$h$). Specifically, $\bar{F}_r$ and $\bar{h}_r$ are given as follows:

$$\bar{F}_r = \frac{\sum_{s:(r,s)\in W} (T_{rs}^o + \epsilon^o) F_{rs}}{\sum_{s:(r,s)\in W} (T_{rs}^o + \epsilon^0)}, \bar{h}_r = \frac{\sum_{s:(r,s)\in W} (T_{rs}^o + \epsilon^o) h_{rs}}{\sum_{s:(r,s)\in W} (T_{rs}^o + \epsilon^o)}, \forall\, r \in R, \tag{3}$$

where T_{rs}^o is the occupied RV flow that serves customer demand from node r to s; the small constant ϵ^0 is applied to ensure the feasibility of mapping in case $\sum_{s:(r,s)\in W} T_{rs}^o$ in the denominator is zero. Nevertheless, this treatment is primarily for mathematical completeness. Online Appendix B shows that the zero-flow condition will arise along with an infinite long wait for RVs (i.e., $w_r^v \to +\infty$). In this case, the items $\bar{F}_r$ and $\bar{h}_r$ weighted from F_{rs} and h_{rs}, respectively, become negligible among the utility specification (2).

Assume that each idle RV cruises toward a node $r \in R$ that maximizes its perceived utility and that the perception error on the utility follows the Gumbel distribution. Then, the portion of idle RVs cruising to r among all those generated at node s, denoted as P_{sr}, is given

$$P_{sr} = \frac{\exp(\theta U_{sr})}{\sum_{k\in R} \exp(\theta U_{sk})}, \quad \forall\, s \in S, r \in R,$$

Table 1. Notation List of Sets, Variables, Parameters, and Functions

Notation	Description
Sets	
V	Set of nodes
A	Set of links
R	Set of the origin nodes of customer trips; $R \subseteq V$
S	Set of the destination nodes of customer trips; $S \subseteq V$
W	Set of OD pairs of ride-sourcing customer demands
W^b	Set of OD pairs of background regular traffic
W^c	Complete set of OD pairs, including those of RVs and regular vehicles
$M^c(r)$	Set of nodes hailing customers at node $r \in R$ can potentially be matched to
L	Set of nodes with positive accumulations of idle RVs
$M^v(l)$	Set of nodes idle RVs at node $l \in L$ can potentially be matched to
Variables	
C_{rs}	Monetary travel cost between OD pair $(r,s) \in W$
F_{rs}	Fare of a trip from node r to s
w_r^c	Customer's average waiting time at node r, $r \in R$
h_{rs}	Equilibrium or shortest vehicular travel time between node r and s
Q_{rs}	Customer demand between OD pair $(r,s) \in W$
$U_{sr}(U_{sl})$	Idle RVs' utility of cruising from node $s \in S$ to $r \in R(l \in L)$
$w_r^v(w_l^v)$	Idle RVs' average matching time at node $r \in R(l \in L)$
$\bar{F}_r$	Average fare of customer trips originating from node $r \in R$
$\hat{F}_l$	Average earnings of RVs that get matched at node $l \in L$
$\bar{h}_r$	Average service time of customer trips originating from node $r \in R$
$\hat{h}_l$	Average service time of RVs that get matched at node $l \in L$
T_{rs}^o	Occupied RV flow that serves customer demand from node r to s, $(r,s) \in W$
$T_{sr}^v(T_{sl}^v)$	Idle RV flow from node $s \in S$ to $r \in R(l \in L)$
T_{sr}^n	Regular traffic flow from node r to s, $(r,s) \in W^b$
$N_r^v(N_l^v)$	Number of idle RVs at node $r \in R(l \in L)$
N_r^c	Number of hailing customers at node $r \in R$
T_{lr}^m	Rate of RVs matched from node $l \in L$ to $r \in M^v(l)$
Parameters	
β^o	Customer's out-of-vehicle value of time ($/$h)
β^i	Customer's in-vehicle value of time ($/$h)
γ	RVs' value of time $/$h
θ	Degree of RV drivers' perception error dispersion
N	Total number of RVs in the network
Functions	
f_{rs}	Function of customer demand vs. travel costs for OD pair $(r,s) \in W$
g_{rs}	Function of trip fare vs. travel time for OD pair $(r,s) \in W$
m_r	Aggregate matching function for node $r \in R$
$\Phi^v(\Phi^c)$	Node potential function on accumulations of idle RVs (hailing customers)
Δ	Potential difference function for paired nodes with positive matching flows

where θ is a constant representing the degree of perceptual dispersion. This leads to the corresponding idle RV flow T^v_{sr}, written as

$$T^v_{sr} = \frac{\exp(\theta U_{sr})}{\sum_{k\in R}\exp(\theta U_{sk})} \cdot \sum_{k:(k,s)\in W} T^o_{ks}, \ \forall\, s \in S, r \in R. \tag{4}$$

We note that the search model considers only the service opportunities at the target zones because idle drivers are assumed to reach the zones and then become available for matching there. This, however, could be a strong assumption, because in reality, idle drivers may be matched during the transition when they sweep across zones. Relaxing the assumption requires, for example, the adoption of a sequential search model where idle drivers sequentially update their target zones from the neighboring nodes based on their current locations. A new equilibrium framework that incorporates such a search model is worthy of investigation in the future.

2.3. Intranode Matching Between Hailing Customers and Idle RVs

As mentioned, the base model considers only intranode matching (i.e., customers can only be matched to idle RVs at the same node). Throughout the paper, we assume one customer is matched with one idle RV and thus, do not consider ride pooling. Because each node features an isotropic zone, an aggregate matching function m_r can be used to characterize the matching frictions between unmatched RVs and customers (e.g., Douglas 1972). In particular, we adopt the matching function suggested by Yang and Yang (2011) to capture the competition among drivers and customers over intranode matching:

$$O^m_r = m_r(N^v_r, N^c_r), \ \forall\, r \in R, \tag{5}$$

where O^m_r represents the realized rate of matching at node r; N^v_r and N^c_r denote the number of idle RVs and hailing customers at node r, respectively.

Under steady states, the variables in the matching function are also subject to the following relationships:

$$N^v_r = \left(\sum_{s\in S} T^v_{sr}\right) w^v_r \tag{6a}$$

$$N^c_r = \left(\sum_{s:(r,s)\in W} Q_{rs}\right) w^c_r \tag{6b}$$

$$O^m_r = \sum_{s:(r,s)\in W} T^o_{rs} = \sum_{s:(r,s)\in W} Q_{rs} = \sum_{s\in S} T^v_{sr}. \tag{6c}$$

2.4. Network Equilibrium Under Intranode Matching

Given all the relations regarding idle and occupied RV movements, we define the network equilibrium state that results from interactions between idle and occupied RVs and the background regular traffic generated by nonsharing vehicles. Define W^b as the set of OD pairs for the regular traffic and W^c as the complete set of OD pairs, including those for idle RVs and occupied RVs as well as regular traffic (i.e., $W^c = \{(s,r)|s \in S, r \in R\} \cup W \cup W^b$). Let N denote the total number of RVs serving the network, and let T^n_{rs} denote the OD demand of regular vehicular traffic from node r to s, which in this study, is assumed to be fixed for all $(r,s) \in W^b$. Then, the equilibrium link flow distribution $\{x^{rs}_{ij}\}$ solves the following system of equalities and inequalities:

Path equilibration between OD pairs

$$\left[t_{ij}(v_{ij}) - \rho^{rs}_i + \rho^{rs}_j\right] x^{rs}_{ij} = 0 \qquad \forall\, (i,j) \in A, (r,s) \in W^c \tag{7a}$$

$$t_{ij}(v_{ij}) - \rho^{rs}_i + \rho^{rs}_j \geq 0 \qquad \forall\, (i,j) \in A, (r,s) \in W^c \tag{7b}$$

$$v_{ij} = \sum_{(r,s)\in W^c} x^{rs}_{ij} \qquad \forall\, (i,j) \in A \tag{7c}$$

$$x^{rs}_{ij} \geq 0 \qquad \forall\, (i,j) \in A, (r,s) \in W^c \tag{7d}$$

$$T^{rs} = T^v_{rs} + T^o_{rs} + T^n_{rs} \qquad \forall\, (r,s) \in W^c \tag{7e}$$

$$\sum_{i:(i,k)\in A} x^{rs}_{ik} - \sum_{j:(k,j)\in A} x^{rs}_{kj} = \begin{cases} -T^{rs}, & \text{if } k = r \\ T^{rs}, & \text{if } k = s \\ 0, & \text{otherwise} \end{cases} \qquad \forall\, (r,s) \in W^c \tag{7f}$$

$$h_{rs} = \rho^{rs}_r - \rho^{rs}_s \qquad \forall\, (r,s) \in W^c \tag{7g}$$

Customer demands

$$Q_{rs} = f_{rs}\left(\beta^o w^c_r + (\beta^i + \beta^f) h_{rs}\right) \qquad \forall\, (r,s) \in W \tag{7h}$$

$$F_{rs} = F^0_{rs} + \beta^f h_{rs} \qquad \forall\, (r,s) \in W \tag{7i}$$

Idle RV movements

$$U_{sr} = \bar{F}_r - \gamma \cdot (\bar{h}_r + h_{sr} + w^v_r) \qquad \forall\, s \in S, r \in R \tag{7j}$$

$$\bar{F}_r = \frac{\sum_{s:(r,s)\in W} (T^o_{rs} + \epsilon^o) F_{rs}}{\sum_{s:(r,s)\in W} (T^o_{rs} + \epsilon^o)} \qquad \forall\, r \in R \tag{7k}$$

$$\bar{h}_r = \frac{\sum_{s:(r,s)\in W} (T^o_{rs} + \epsilon^o) h_{rs}}{\sum_{s:(r,s)\in W} (T^o_{rs} + \epsilon^o)} \qquad \forall\, r \in R \tag{7l}$$

$$T^v_{sr} = \begin{cases} \dfrac{\exp(\theta U_{sr})}{\sum_{k\in R}\exp(\theta U_{sk})} \cdot \sum_{k:(k,s)\in W} T^o_{ks}, & \forall\, s \in S, r \in R \\ 0, & \forall\, (s,r) \in W^c \backslash \{(s,r)|s \in S, r \in R\} \end{cases} \tag{7m}$$

Internode matching

$$\sum_{s:(r,s)\in W} T^o_{rs} = M_r\left(\left(\sum_{s\in S} T^v_{sr}\right) w^v_r, \left(\sum_{s:(r,s)\in W} Q_{rs}\right) w^c_r\right) \qquad \forall\, r \in R \tag{7n}$$

$$\sum_{s\in S} T^v_{sr} = \sum_{s:(r,s)\in W} Q_{rs} \quad \forall r \in R \tag{7o}$$

$$T^o_{rs} = \begin{cases} Q_{rs}, & \forall\,(r,s) \in W \\ 0, & \forall\,(r,s) \in W^c \backslash W \end{cases} \tag{7p}$$

RV fleet conservation

$$\sum_{(r,s)\in W} T^o_{rs} h_{rs} + \sum_{(s,r):s\in S, r\in R} T^v_{sr} \cdot (h_{sr} + w^v_r) = N, \tag{7q}$$

where $\{\rho^{rs}_k\}$ are auxiliary variables and $\{t_{ij}\}_{(i,j)\in A}$ denote link performance functions that increase monotonically on the corresponding link flows. Note that the number of RVs N is assumed to be fixed, known to the transportation planning agencies. However, if drivers' opportunity wage is available, it is straightforward to relax this assumption by introducing a function that relates the fleet size to the effective income of drivers. A similar treatment can also be done for the background traffic demand to capture its elasticity on the travel time. The solution algorithm introduced in Section 4.4 can be readily adapted to incorporate these extensions. In addition, the model assumes that drivers always take the routes with minimum travel time. In practice, drivers may be concerned about other costs such as fuel consumption and wearing that are primarily distance-based. In this case, a generalized cost function can be introduced to encapsulate the distance-based cost component for route choice. Consequently, when deciding where to search for customers, RV drivers will consider the generalized travel cost.

The existence of equilibria for the nonlinear complementarity system (7) is proved in Online Appendix B, as the special case of the system under internode matching, which is introduced in Section 3.

3. Modeling Internode Matching Between Customers and Idle RVs

The base model captures the matching of customers and drivers within a small neighborhood. However, because of the spatial heterogeneity in the ride-sourcing markets, platforms frequently match idle RVs from one area with excessive supply to customers at another area experiencing supply shortage. As a consequence, RVs are often matched to customers who are several miles away. Modifications should be made to handle this type of long-distance spatial matching, which appears to be a common practice by ride-sourcing platforms.

One straightforward remedy is to enlarge each node to cover a relatively large area with internally balanced demand and supply. However, such an evading strategy may compromise the representativeness and accuracy of the established model, as the aggregate matching function is likely to be biased if intranode heterogeneity is left out. More importantly, as the node "grows" larger, the intranode traffic becomes substantial and comparable with the internode traffic, defeating the original intent of conducting a network equilibrium analysis.

We thus resort to explicit modeling of the long-distance matching among different nodes while keeping the node itself to be isotropic and at the neighborhood scale. For passengers at node $r \in R$, we use $M^c(r)$ to represent the set of nodes whose idle RVs can be potentially matched to them. Let $L = \cup_{r\in R} M^c(r)$. Note that these matching sets are not mutually exclusive. Reversely, there is also another matching set $M^v(l) \subseteq R$ for idle RVs at each $l \in L$, representing the set of nodes whose passengers can be matched with idle RVs at l. In this study, we assume that all matching sets $\{M^c(r)\}$ and $\{M^v(l)\}$ are exogenously predetermined and then, use T^m_{lr} to denote the rate of RVs matched from node $l \in L$ to $r \in M^v(l)$.[1]

3.1. Challenges in Modeling Internode Matching

Previously, the intranode matching flow is estimated from the number of hailing customers and idle vehicles at the same node using a single-output matching function. With internode matching, the idle vehicles/hailing customers at each node can possibly be matched to customers/RVs at a set of nodes. Consequently, a multioutput matching function must be developed to delineate aggregately the matching process. Figure 1(a) outlines a conceptual instance for internode matching, where the blue circles on the left and the green circles on the right represent the pools of idle RVs and hailing customers at different nodes, respectively. Let N^v_l and N^c_r denote the average number of entities at nodes $l \in L$ and $r \in R$, respectively, under the steady state. Then, as shown in Figure 1(a), the RV accumulations N^v_1 at node 1 are "digested" by flows T^m_{11} and T^m_{12}, whereas the customer accumulations N^c_1 are matched to generate flows of T^m_{11} and T^m_{21}, etc. Therefore, when determining T^m_{11}, the knowledge on N^v_1 and N^c_1 is not sufficient. We also must know flows such as T^m_{12} and T^m_{21}, which may further depend on $\{T^m_{2r}\}$ and $\{T^m_{l2}\}$, etc. Propagating by nodes and links, the interdependencies are likely to integrate over the whole set of matching flows $\{T^m_{lr}\}_{l\in L, r\in R}$ throughout a well-connected network.

Another challenge arises from the matching priority issue. Taking Figure 1(a) as an example, there are two possible matching outcomes for RVs in N^v_1, either node 1 or 2. Suppose customer requests from node 1 can be served by RVs from the same node with shorter pickup time, compared with the counterparts at node 2. Then, idle RVs at node 1 will be prioritized to match with closer customers (i.e., the customers at node 1 in this case). The modeling of such a priority is nontrivial because the comparative nature of priorities essentially gives rise to asymmetries for the paired nodes as well as the interdependencies between pairs.

Figure 1. (Color online) Analogy of (a) Internode Matching Flows to (b) Currents in an Electric Circuit

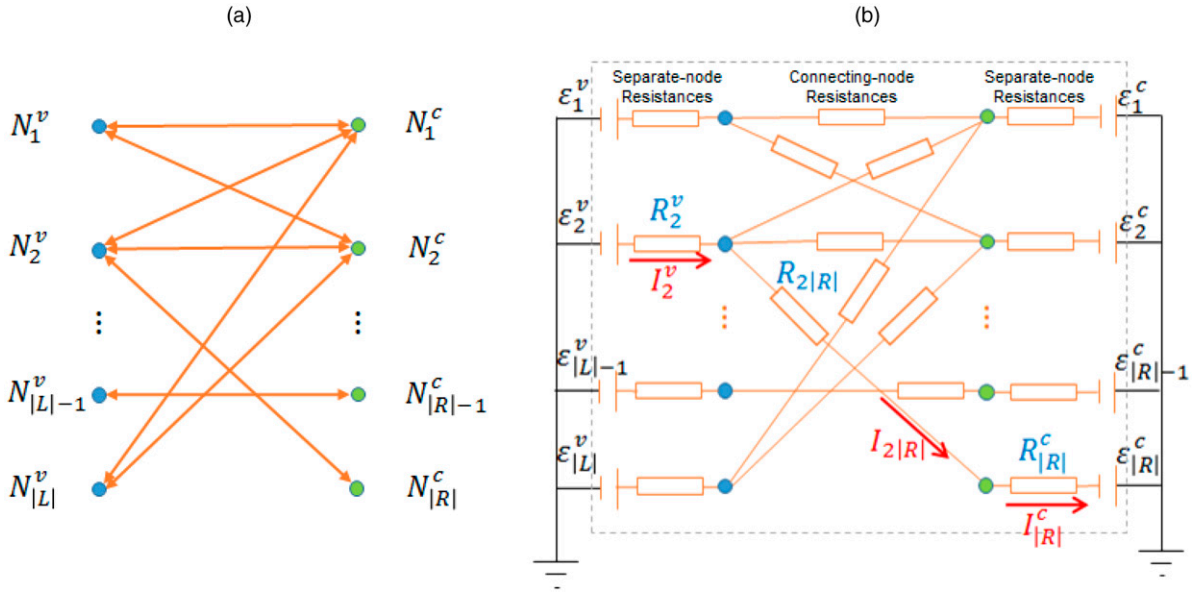

3.2. Internode Matching Functions

Our internode matching function is built on an analogy to electric circuits. For each internode matching graph (e.g., Figure 1(a)), a corresponding electric circuit can be constructed by duplicating the connections with resistances (also known as connecting-node resistance) (see Figure 1(b)). Additionally, each node outstretches a separate resistance (also known as separate-node resistance) as well as an external power supply and connects in parallel to constitute a circuit. Denote ε_i^t, R_i^t, and I_i^t as the power voltage, the resistance, and the current on each node's individual branch, respectively, where

$$\{(t,i)|t \in \{v,c\}; i \in L, \text{if } t = v; i \in R, \text{if } t = c\}.$$

Denote R_{lr} and I_{lr} as the resistance and the current, respectively, on connections between the paired nodes l and r, where $l \in L$ and $r \in R$. Then, the currents on the graph are subject to the following relationships as per Kirchhoff's circuit laws:

$$(\varepsilon_l^v - R_l^v \cdot I_l^v) - (R_r^c \cdot I_r^c - \varepsilon_r^c) = R_{lr} \cdot I_{lr}, \quad \forall\, (l,r) \in \{(l,r)|r \in M^v(l), l \in L\} \tag{8a}$$

$$I_l^v = \sum_{r \in M^v(l)} I_{lr}, \quad \forall\, l \in L \tag{8b}$$

$$I_r^c = \sum_{l \in M^c(r)} I_{lr}, \quad \forall\, r \in R. \tag{8c}$$

The two terms on the left-hand side of Equation (8a) represent the potentials at the left and right circles, whereas the right-hand side calculates the potential difference in terms of Ohm's law. The latter two equations (Equations (8b) and (8c)) essentially represent current conservation at nodes. We hypothesize that such an electric circuit framework mimics or approximates the internode matching process and its outcomes. The current on each branch of the circuit is analogous to the matching flow between the corresponding paired nodes, and the voltage of each power supply measures the accumulation of entities at the corresponding node. For each individual branch, higher voltage/accumulation will yield larger current/flow. Further, the resistances in the electric circuit characterize the time that RVs/customers spend during each process. Specifically, the separate-node resistance represents the waiting time of RVs/customers at each node, whereas the connecting-node resistance quantifies the RVs' deadheading or pickup time for customers in between. The interdependencies of currents/flows thus transmit rotationally through the two types of resistances/residence time and propagate systematically to the whole graph.

In light of the analogy, we construct the internode matching function following a similar principle. Denote ϕ_l^v and ϕ_r^c as the matching potentials of RVs and customers that wait at different nodes, respectively, and define them as the functions[2]

$$\phi_l^v = \log\left(\Phi^v(T_l^v, N_l^v)\right), \qquad \forall\, l \in L$$

$$\phi_r^c = -\log\left(\Phi^c(T_r^c, N_r^c)\right), \qquad \forall\, r \in R,$$

where the potential function Φ (including Φ^v and Φ^c) ranges in $(0, +\infty)$, decreasing on the cumulative flow T and increasing on the accumulation N (i.e., $\frac{\partial \Phi}{\partial T} < 0$ and $\frac{\partial \Phi}{\partial N} > 0$). Note that the waiting time w does not appear in Φ's variable argument list because in this case, w can be directly written as a function of N over T. In addition, we define the potential difference on each

pair of connected nodes as the flow and travel time in between: that is,

$$\delta\phi_{lr} = \log\left(\Delta(T^m_{lr}, h_{lr})\right),$$
$$\forall\ (l,r) \in \{(l,r) | r \in M^v(l), l \in L\},$$

where the function Δ also ranges from $(0, +\infty)$, and $\frac{\partial \Delta}{\partial T^m} > 0$, $\frac{\partial \Delta}{\partial h} > 0$.

Then, by setting the accumulations $\{N^v_l\}$, $\{N^c_r\}$ and node-transfer time $\{h_{lr}\}$ as given parameters, the resultant matching flow pattern $\{T_{lr}\}$ in line with Equation (8) solves the equation system[3]

$$\Phi^v(T^v_l, N^v_l) \cdot \Phi^c(T^c_r, N^c_r) = \Delta(T^m_{lr}, h_{lr}), \quad \forall\ (l,r) \in \{(l,r) | r \in M^v(l), l \in L\} \tag{9a}$$

$$T^v_l = \sum_{r \in M^v(l)} T^m_{lr}, \qquad \forall\ l \in L \tag{9b}$$

$$T^c_r = \sum_{l \in M^c(r)} T^m_{lr}, \qquad \forall\ r \in R. \tag{9c}$$

We assume the functions $\Phi(T,N)$, including Φ^v and Φ^c, as well as $\Delta(T,h)$ additionally satisfy the following properties (with implications clarified), given any N and h with positive and finite values.

- Domain of definition. Both $\Phi(T,N)$ and $\Delta(T,h)$ are continuous functions defined on $T \in (0, +\infty)$. For each pair of nodes with one located in the matching range of the other, there will be positive flows matched in between.
- Boundary conditions. First, $\lim_{T \to 0^+} \Phi(T,N) = +\infty$ and $\lim_{T \to +\infty} \Phi(T,N) = 0$. These two conditions can be obtained conceptually, as the accumulation N is stuck in the matching process when $T \to 0^+$ and dissipates instantaneously for $T \to +\infty$. Second, $\lim_{T \to 0^+} \Delta(T,h) = 0$ and $\lim_{T \to +\infty} \Delta(T,h) = +\infty$. As per the Ohm's law, fewer potential differences are associated with fewer matching flows through the time impedance.
- Limiting behavior. There exist $p > 0$ and $q > 0$ such that[4]

$$\Phi(T,N) = \begin{cases} \Theta(T^{-p}), & \text{as } T \to 0^+ \\ \Theta(T^{-q}), & \text{as } T \to +\infty \end{cases}.$$

This implies a diminishing marginal rate of substitution in the matching process. We let Φ possibly converge/grow on T with different speed when approaching $0^+ / +\infty$, respectively.

Based on these general properties on Φ and Δ, the existence and uniqueness of solutions $\{T^m_{lr}\}$ to system (9) are proven in Online Appendix A. Also, it is worth pointing out that when the exogenous matching range of each node confines to itself, the derived internode matching functions degenerate to an intranode counterpart: that is,

$$\Phi^v(T^m_{rr}, N^v_r) \cdot \Phi^c(T^m_{rr}, N^c_r) = \Delta(T^m_{rr}, h_{rr}),$$

Figure 2. (Color online) Maps for the Target District in Changsha, China

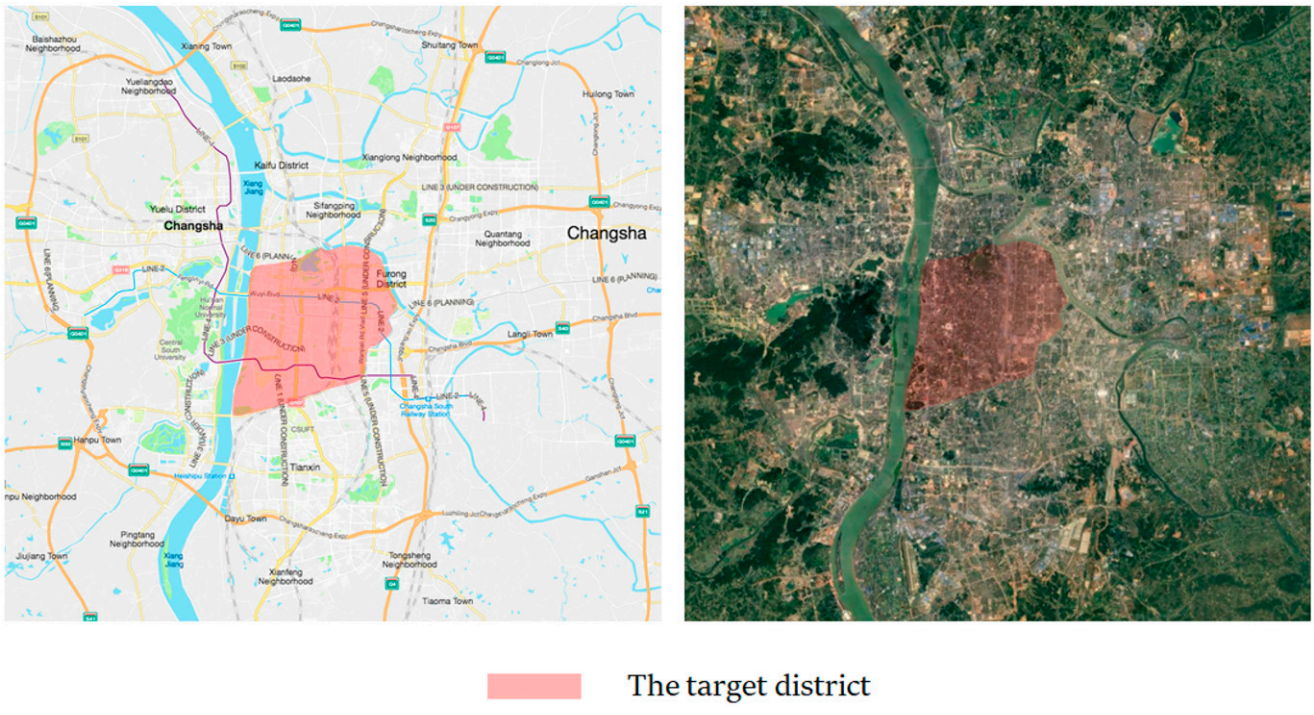

which incorporates the specification of Yang and Yang (2011) as a special case.

3.3. Empirical Validation of the Internode Matching Functions

We now apply an empirical data set from Didi Chuxing to demonstrate the effectiveness of the proposed internode matching function. The data set contains service states of all customers and drivers in the central district of Changsha, China (see Figure 2 for a map of the district) during the whole year of 2019. The region covers an area of about 60 km^2 and consists of 50 standard hexagonal zonal partitions.[5] We aggregate the data by one-hour intervals between 7:00 and 22:00 each day to produce samples required by the proposed matching functions. Each sample then records the number of rider-driver matches and the average pickup time between two zones, as well as the total drivers and riders' flows and accumulations at each zone. Figure 3 visualizes the interzonal matching flows in this area. The horizontal and vertical axes list the 50 hexagonal zones where waiting customers and idle drivers stay, respectively. Each box intersected by a column and a row visualizes the yearly number of matches between the corresponding pair of zones. As shown in the figure, a significant portion of matches takes place interzonally under the 660-meter hexagon partitions, which an intrazonal matching function may fall short of modeling. The empirical analysis further demonstrates the necessity of an interzonal matching model and validates the effectiveness of the one we propose.

Let the potential functions Φ^v, Φ^c and the potential difference function Δ in Equation (9a) all take the product forms as follows:

$$\Phi^v(T_l^v, N_l^v) = T_l^{vq_T^v} \cdot N_l^{vq_N^v}$$

$$\Phi^c(T_r^c, N_r^c) = T_r^{cq_T^c} \cdot N_r^{cq_N^c}$$

$$\Delta(T_{lr}^m, h_{lr}) = \eta_{lr}^{-1} \cdot T_{lr}^m \cdot F(h_{lr})^{-1},$$

where $\boldsymbol{\eta}$ and $\boldsymbol{q}$ are parameters; $F(\cdot)$ specifies a univariate function of the interzonal travel time. Substituting Φ^v, Φ^c, and Δ in Equation (9a) with their correspondences and then taking logarithms yield

$$\log T_{lr}^m = \log \eta_{lr} + \log F(h_{lr}) + q_T^v \cdot \log T_l^v + q_N^v \cdot \log N_l^v + q_T^c \cdot \log T_r^c + q_N^c \cdot \log N_r^c,$$

which is invited as the basis for our empirical validation.

Figure 3. (Color online) Interzonal Matching Between Riders and Drivers

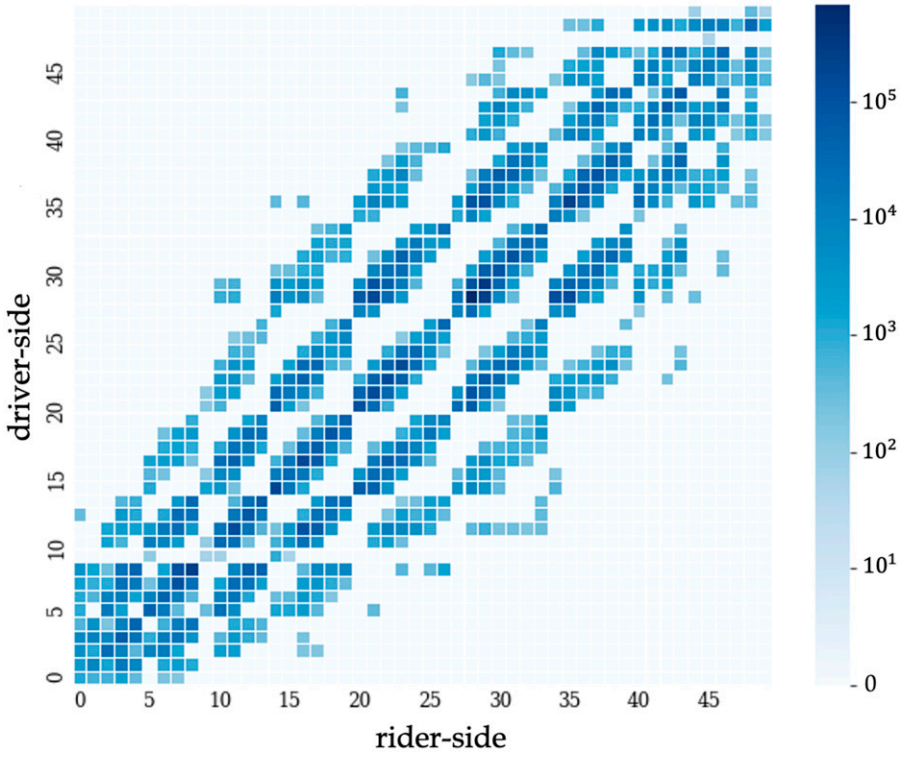

Notes. The horizontal and vertical axes array the 50 zones where riders and drivers stay before being matched, respectively. Each box intersected by a column and a row visualizes the number of matches realized between the pair of zones. Specifically, the boxes laid on the diagonal from the lower left to the upper right count the intrazonal matches. Darker colors indicate larger numbers of riders and drivers being matched.

The following model is constructed for regression analysis:

$$\begin{aligned}\log T^m_{lr,t} &= \alpha_{lr} + \beta_t + \gamma_{lr,t} + q^v_N \cdot \log N^v_{l,t} + q^c_N \cdot \log N^c_{r,t} \\ &+ q^v_T \cdot \log T^v_{l,t} + q^c_T \cdot \log T^c_{r,t} + q_h{}' \cdot \log h_{lr,t} + q_h{}'' \cdot h_{lr,t} \\ &+ q_h{}'' \cdot h^2_{lr,t} + \mathbf{1}_{\text{intra}} \times (d + d^v_N \cdot \log N^v_{l,t} + d^c_N \cdot \log N^c_{r,t} \\ &+ d^v_T \cdot \log T^v_{l,t} + d^c_T \cdot \log T^c_{r,t}) + \epsilon_{lr,t}, \end{aligned} \tag{10}$$

where the subscript t denotes the time stamp of each sample; the interzonal (α_{lr}) and time (β_t) fixed effects are incorporated to control for influences that are constant either over time or across zonal pairs, respectively. We spell the time fixed effects as a series of indicators for hour of week and week of year, as well as national holidays; $\gamma_{lr,t}$ is a set of controls that vary over both space and time. Meanwhile, the real-time weather information, including the temperature, humidity, precipitation intensity, fine particulate matter (PM 2.5) level, wind speed, and sky condition in the region, is also incorporated to control the latent impacts on the system. The effects of spatial distance h_{lr} in matching are captured using three terms: $\log h_{lr}$, h_{lr}, and h^2_{lr}. Special considerations are given to the within-zonal matching to allow certain differentiation from the matching between two different zones. We denote $\{\boldsymbol{q}, \boldsymbol{d}\}$ as two sets of coefficients to the various factors.

Based on the construction (10), we calibrate five degenerated models (see Table 2) for comparison. Model M1 captures only the fixed effects from space, time, and weather, etc. without using state variables from the ride-sourcing system. Model M2 additionally involves the number of idle drivers and customers accumulated at each zone, adapting the existing aggregate matching function of street-hailing taxi systems. Model M3 characterizes a basic one that comes into our internode matching category, whereas Model M4 provides extra freedom for within-zonal matching. Model M5 is a parsimonious internode matching model that abandons all the controls and retains only the essential system-state variables. Comparisons across the five models help disclose the completeness of different sets of factors in determining the interzonal matching.

Additionally, it is worth noting that among the samples of all the effective zonal pairs,[6] only 2% contain more than 20 matches within the hourly slot. Such an extreme concentration of samples causes noises to dominate the variation of the predicting matching volumes and thus, substantially troubles the regression, yielding ineffective model fitting (see Qu, Wang, and Zhang 2015 for a relevant discussion). To resolve such an issue, we truncate the samples by trimming those with an hourly number of matches $T^m_{lr,t}$ less than 20 and then apply the rest (77,016 records in total) to calibrate the internode matching models using truncated regression. The samples are further divided into two for training and testing purposes. Because Models M1–M4 involve various spatio-temporal fixed effects, we allocate the set of samples produced in the northern district (to the north of latitude 28°11′ N) in the second half of the year 2019 for testing and retain the other samples as the training set (see Figure 4 for the details).

The validation results are summarized in Table 2, where the bottom five rows present a set of performance metrics that evaluate the five models over the truncated samples. As clearly shown, the models are significantly improved as we enrich the variable specifications from Model M1 to Model M4. Specifically, the internode matching models with a complete set of variables specified consistently outperform the existing

Table 2. Comparison of Five Regression Models for Interzonal Matching

	M1		M2		M3		M4		M5	
Fixed effects and controls	✓		✓		✓		✓			
$\{\boldsymbol{N}^v, \boldsymbol{N}^c\}$			✓		✓		✓		✓	
$\{\boldsymbol{T}^v, \boldsymbol{T}^c, \boldsymbol{F}(\boldsymbol{h})\}$					✓		✓		✓	
$1_{\text{intra}} \times \{1, \boldsymbol{N}^v, \boldsymbol{N}^c, \boldsymbol{T}^v, \boldsymbol{T}^c\}$							✓		✓	
Degrees of freedom	130		128		128		127		12	
Data set (train: 37,145; test: 39,871)	Train	Test	Train	Test	Train	Test	Train	Test	Train	Test
Explained variance $1 - \text{Var}(\boldsymbol{y}-\hat{\boldsymbol{y}})/\text{Var}(\boldsymbol{y})$	0.643	0.607	0.732	0.727	0.925	0.935	0.942	0.943	0.916	0.923
R^2 score $1 - \sum_{i=1}^{n}(y_i - \hat{y}_i)^2 / \sum_{i=1}^{n}(y_i - \bar{y})^2$	0.542	0.516	0.676	0.681	0.919	0.931	0.939	0.940	0.907	0.921
Mean absolute error $\sum_{i=1}^{n}\lvert y_i - \hat{y}_i\rvert/n$	12.28	15.13	10.28	12.19	5.29	6.21	4.62	5.78	5.86	6.81
Mean squared error $\sum_{i=1}^{n}(y_i - \hat{y}_i)^2/n$	305.0	553.5	215.7	364.3	53.9	78.4	40.9	68.6	62.0	90.0
Correlation $\text{cov}(\boldsymbol{y}, \hat{\boldsymbol{y}})/(\sigma_y \sigma_{\hat{y}})$	0.802	0.789	0.856	0.863	0.962	0.968	0.971	0.971	0.957	0.961

Notes. Truncated regressions are performed on the training set with hourly matching volumes higher than 20 between two zonal pairs. Results on both training and testing sets are presented using five performance metrics by comparing the predicted ($\hat{\boldsymbol{y}}/\{\hat{y}_i\}$) and observed ($\boldsymbol{y}/\{y_i\}$) numbers of interzonal matches over the sample (of size n). The item $\bar{y}$ denotes the sample mean of $\boldsymbol{y}$.

Figure 4. (Color online) Division of Training and Testing Sets

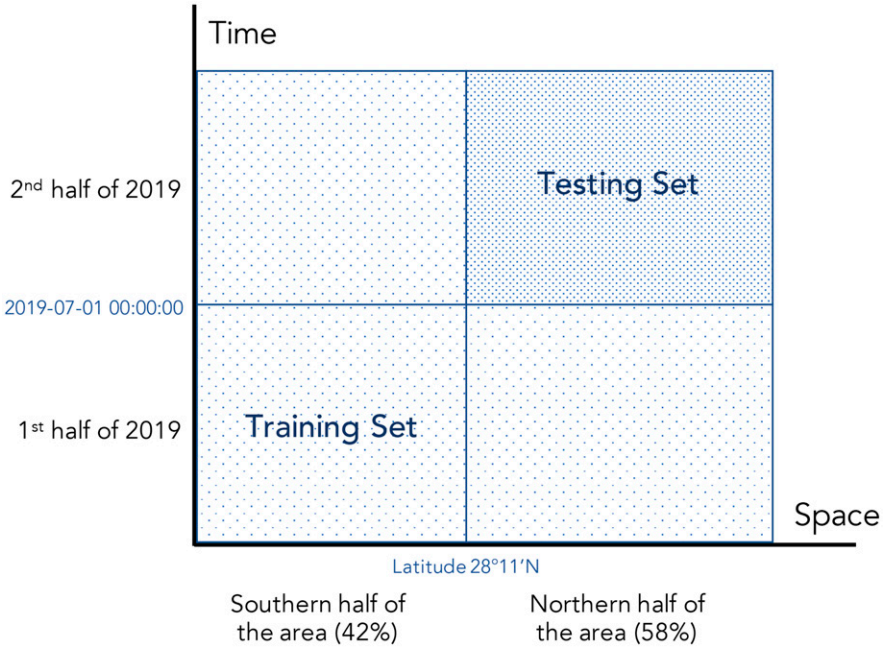

Note. The testing set constitutes those samples that originated from the northern part of the target district (to the north of latitude 28°11′ N) in the second half of 2019, whereas the training set consists of the rest.

intranode model developed for street-hailing taxis, which is surely better than the one without considering market information. Meanwhile, Model M5, which keeps only the most core set of covariates, provides a prediction level equivalent to the sophisticated models, Models M4 and M5. This implies that the structure of our model adheres well to the intrinsic physics of the matching process managed by the platform, regardless of its variations in time, space, and weather, etc.

The results validate the representativeness of our model for interzonal matching at the high-volume regime. However, as mentioned, about 98% of the samples contain only very few matches over the hourly periods. Figure 5 compares the predicted versus observed numbers of matches over the complete sample from the effective zonal pairs by using the calibrated models. Overall, the set of figures suggests highly consistent results with the truncated sample analysis, assuring the generalization of our proposed model. Specifically, Model M2, which is originally applied for the taxi market, largely underestimates the number of matches in the high-volume regime. The internode matching model, Model M3, fixes such an underestimation significantly, whereas Model M4 with additional differentiation for intrazonal matching provides the highest consistency between the predicted and observed matching volumes. Again, the parsimonious model, Model M5, is able to achieve a similar level of prediction precision as Model M4.

In summary, the empirical validation proves the potential of our modeling framework as a scalable recapitulation for internode matching. However, it is worth noting that the calibrated models are yet not ready for parametric interpretation, as the parameters may not take the physical meaning as they should be in the model construction. The covariates are not fully identified under the current setting because of the nature of endogeneity amongst the flows and accumulations of drivers and riders. Notwithstanding, the comparisons between the predicted and the observed matching volumes do endorse our model specifications as well as the comprehensiveness of factors that we consider for internode matching. For future implementations, designated experiments could be conducted to inference the causal relationship between the interzonal matching rates and the system states at different zones, so as to systematically calibrate the matching functions.

4. Network Equilibrium Under Internode Matching Condition

With the enhanced matching functions proposed in Section 3, we proceed to relax the intranode matching assumption in the base model to consider the internode matching between customers and idle RVs. The modules of the customer demand and the idle RVs' search movements are first adapted accordingly to the new context.

Figure 5. (Color online) Predicted vs. Observed Number of Matches over the Nontruncated Testing Sample

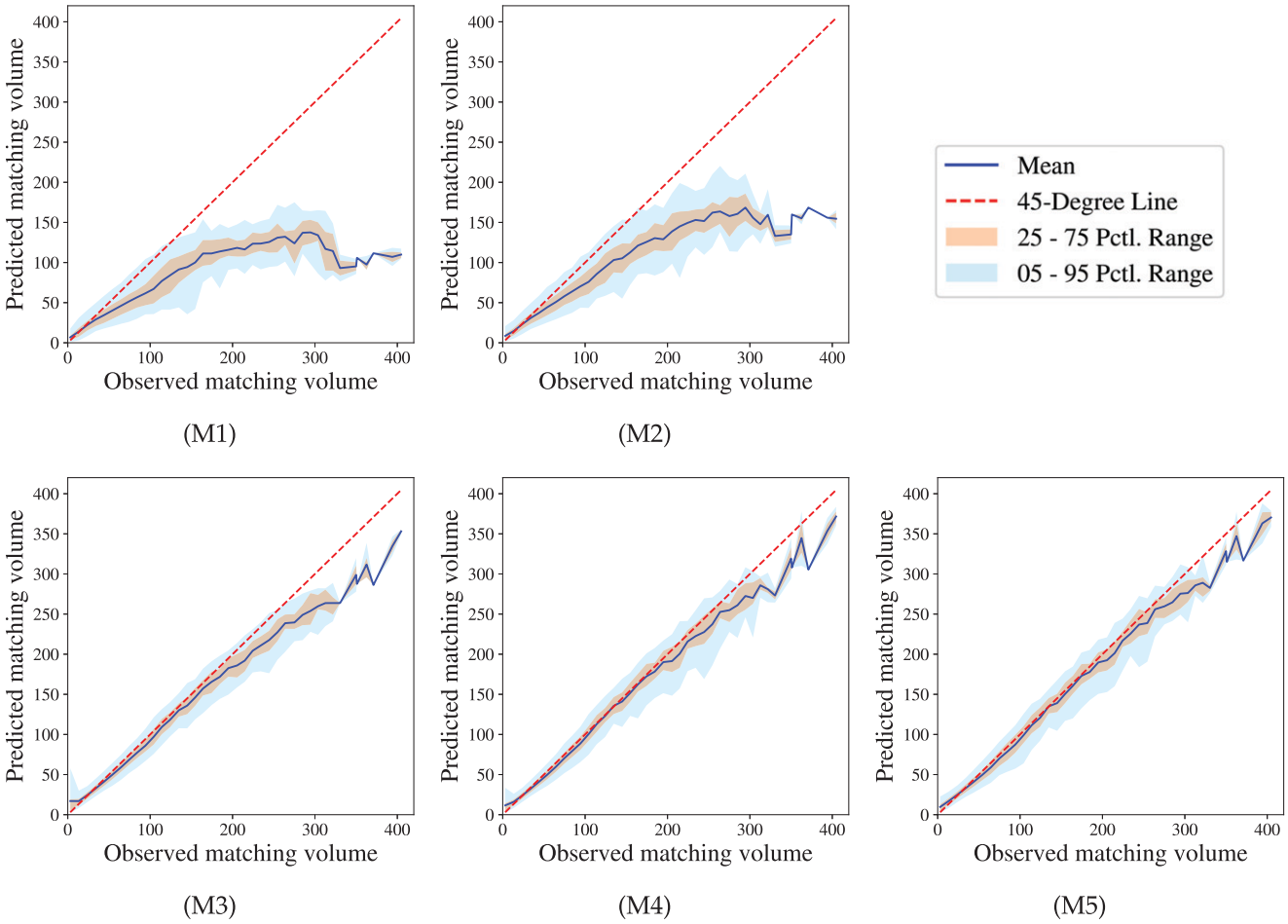

Notes. The solid line in the middle shows the mean predictions of interzonal matching volumes over each level observed, whereas the inner and outer shaded areas graph the [25, 75] and [5, 95] percentile ranges of predictions, respectively. The dotted diagonal presents a 45° line for reference. Pctl., percentile.

4.1. Customer Demand Under Internode Pickups

Customers' travel costs now explicitly embody the internode pickup time:

$$C_{rs} = g_{rs} + \beta^o w_r^c + \beta^m \check{h}_r + (\beta^i + \beta^f) h_{rs}, \ \forall\ (r,s) \in W,$$

where β^m denotes customers' value of the pickup time ($/h) and $\check{h}_r$ is the average internode pickup time for customers on node r:

$$\check{h}_r = \frac{\sum_{l \in M^c(r)} (T_{lr}^m + \epsilon^m) h_{lr}}{\sum_{l \in M^c(r)} (T_{lr}^m + \epsilon^m)}, \ \forall\ r \in R. \tag{11}$$

The small constant ϵ^m features another treatment defined to ensure the feasibility of mapping (11) when all the flow T_{lr}^m values are zero. We note that the use of ϵ^m here is also innocuous because the zero-flow condition essentially arises when w_r^c approaches infinity, under which any $\check{h}_r$ valued from the convex hull formed by $\{h_{lr}\}$ becomes nil in comparison.

The customer demand Q_{rs} is then subject to a function reformulated as follows:

$$Q_{rs} = f_{rs}\left(\beta^o w_r^c + \beta^m \check{h}_r + (\beta^i + \beta^f) h_{rs}\right), \ \forall\ (r,s) \in W.$$

4.2. Idle RVs' Search Target Zones

Although the fundamental behavioral consideration remains the same, the modeling of idle RV movements also must be updated, as drivers now choose their search target nodes based on all the potential matching outcomes, including matches to passengers at other nodes in the matching set of a target node. Therefore, the utility function of an idle RV cruising from node $s \in S$ to any node $l \in L$ is respecified as

$$U_{sl} = \hat{F}_l - \gamma \cdot (\hat{h}_l + h_{sl} + w_l^v), \ \forall\ s \in S, l \in L,$$

where $\hat{F}_l$ and $\hat{h}_l$ are the average fare and service time of RVs that get matched at node l. Note that the service time now consists of two parts corresponding to

deadheading to pick up the matched passenger and then delivering them. We can expand $\hat{F}_l$ and $\hat{h}_l$, respectively, as follows:

$$\hat{F}_l = \frac{\sum_{r\in M^v(l)} (T^m_{lr}+\epsilon^m)\bar{F}_r}{\sum_{r\in M^v(l)} (T^m_{lr}+\epsilon^m)}, \quad \hat{h}_l = \frac{\sum_{r\in M^v(l)} (T^m_{lr}+\epsilon^m)(h_{lr}+\bar{h}_r)}{\sum_{r\in M^v(l)} (T^m_{lr}+\epsilon^m)}, \ \forall\, l\in L,$$

where $\bar{F}_r$ and $\bar{h}_r$ still follow the previous definitions in Equation (3). By assuming that drivers' perception errors on utilities follow the Gumbel distribution, we then write the idle RV flow T^v_{sl} under the internode matching scenario as

$$T^v_{sl} = \frac{\exp(\theta U_{sl})}{\sum_{k\in L}\exp(\theta U_{sk})}\cdot \sum_{k:(k,s)\in W} T^o_{ks}, \ \forall\, s\in S, l\in L.$$

4.3. Equilibrium Condition

Based on the modifications derived for internode matching, we rewrite the network equilibrium conditions (7) to reflect the impacts of internode matching. In particular, we replace the intranode matching function with the internode counterpart and account for the internode pickups in the cost specifications of customers and drivers' behavioral components. The framework (12) thus characterizes a general equilibrium under internode matching that integrates the ride-sourcing market and network equilibration as well as the interplay between them. The complete set of OD pairs W^c now includes those for idle RV trips, deadheading RV trips, and occupied RV trips as well as trips made by regular traffic: that is,

$$W^c = \{(s,l)|s\in S, l\in L\}\bigcup\{(l,r)|l\in L, r\in M^v(l)\}\bigcup W\bigcup W^b.$$

Then, the equilibrium link flow distribution $\{x^{rs}_{ij}\}$ satisfies the following conditions:

Path equilibration between OD pairs

$$\left[t_{ij}(v_{ij})-\rho^{rs}_i+\rho^{rs}_j\right]x^{rs}_{ij}=0 \qquad \forall\,(i,j)\in A,(r,s)\in W^c \tag{12a}$$

$$t_{ij}(v_{ij})-\rho^{rs}_i+\rho^{rs}_j\geq 0 \qquad \forall\,(i,j)\in A,(r,s)\in W^c \tag{12b}$$

$$v_{ij}=\sum_{(r,s)\in W^c} x^{rs}_{ij} \qquad \forall\,(i,j)\in A \tag{12c}$$

$$x^{rs}_{ij}\geq 0 \qquad \forall\,(i,j)\in A,(r,s)\in W^c \tag{12d}$$

$$T^{rs}=T^v_{rs}+T^m_{rs}+T^o_{rs}+T^n_{rs} \qquad \forall\,(r,s)\in W^c \tag{12e}$$

$$\sum_{i:(i,k)\in A} x^{rs}_{ik}-\sum_{j:(k,j)\in A} x^{rs}_{kj}=\begin{cases}-T^{rs}, & \text{if } k=r\\ T^{rs}, & \text{if } k=s\\ 0, & \text{otherwise}\end{cases} \qquad \forall\,(r,s)\in W^c \tag{12f}$$

$$h_{rs}=\rho^{rs}_r-\rho^{rs}_s \qquad \forall\,(r,s)\in W^c \tag{12g}$$

Customer demands

$$Q_{rs}=f_{rs}\left(\beta^o w^c_r+\beta^m \check{h}_r+(\beta^i+\beta^f)h_{rs}\right) \qquad \forall\,(r,s)\in W \tag{12h}$$

$$\check{h}_r=\frac{\sum_{l\in M^c(r)}(T^m_{lr}+\epsilon^m)h_{lr}}{\sum_{l\in M^c(r)}(T^m_{lr}+\epsilon^m)} \qquad \forall\, r\in R \tag{12i}$$

$$F_{rs}=F^0_{rs}+\beta^f h_{rs} \qquad \forall\,(r,s)\in W \tag{12j}$$

Idle RV movements

$$U_{sl}=\hat{F}_l-\gamma\cdot(\hat{h}_l+h_{sl}+w^v_l) \qquad \forall\, s\in S, l\in L \tag{12k}$$

$$\hat{F}_l=\frac{\sum_{r\in M^v(l)}(T^m_{lr}+\epsilon^m)\bar{F}_r}{\sum_{r\in M^v(l)}(T^m_{lr}+\epsilon^m)} \qquad \forall\, l\in L \tag{12l}$$

$$\hat{h}_l=\frac{\sum_{r\in M^v(l)}(T^m_{lr}+\epsilon^m)(h_{lr}+\bar{h}_r)}{\sum_{r\in M^v(l)}(T^m_{lr}+\epsilon^m)} \qquad \forall\, l\in L \tag{12m}$$

$$\bar{F}_r=\frac{\sum_{s:(r,s)\in W}(T^o_{rs}+\epsilon^o)F_{rs}}{\sum_{s:(r,s)\in W}(T^o_{rs}+\epsilon^o)} \qquad \forall\, r\in R \tag{12n}$$

$$\bar{h}_r=\frac{\sum_{s:(r,s)\in W}(T^o_{rs}+\epsilon^o)h_{rs}}{\sum_{s:(r,s)\in W}(T^o_{rs}+\epsilon^o)} \qquad \forall\, r\in R \tag{12o}$$

$$T^v_{sl}=\begin{cases}\dfrac{\exp(\theta U_{sl})}{\sum_{k\in L}\exp(\theta U_{sk})}\cdot\sum_{k:(k,s)\in W} T^o_{ks}, & \forall\, s\in S, l\in L\\ 0, & \forall\,(s,l)\in W^c\backslash\{(s,l)|s\in S, l\in L\}\end{cases} \tag{12p}$$

$$T^o_{rs}=\begin{cases}Q_{rs}, & \forall\,(r,s)\in W\\ 0, & \forall\,(r,s)\in W^c\backslash W\end{cases} \tag{12q}$$

Internode matching

$$\Phi^v(T^v_l, w^v_l\cdot T^v_l)\cdot\Phi^c(T^c_r, w^c_r\cdot T^c_r)=\Delta(T^m_{lr}, h_{lr}) \quad \forall\, l\in L, r\in M^t(l) \tag{12r}$$

$$T^v_l=\sum_{r\in M^v(l)} T^m_{lr} \qquad \forall\, l\in L \tag{12s}$$

$$T^c_r=\sum_{l\in M^c(r)} T^m_{lr} \qquad \forall\, r\in R \tag{12t}$$

$$\sum_{r\in M^v(l)} T^m_{lr}=\sum_{s\in S} T^v_{sl} \qquad \forall\, l\in L \tag{12u}$$

$$\sum_{l\in M^c(r)} T^m_{lr}=\sum_{s:(r,s)\in W} T^o_{rs} \qquad \forall\, r\in R \tag{12v}$$

$$T^m_{lr}=0, \quad \forall\,(l,r)\in W^c\backslash\{(l,r)|l\in L, r\in M^v(l)\} \tag{12w}$$

RV fleet conservation

$$\sum_{(r,s)\in W^c}(T^o_{rs}+T^v_{rs}+T^m_{rs})\cdot h_{rs}+\sum_{(s,l):s\in S, l\in L} T^v_{sl}\cdot w^v_l=N. \tag{12x}$$

Again, $\{\rho_k^{rs}\}$ are auxiliary variables. The existence of an equilibrium solution to the system (12) is proved in Online Appendix B.[7] As system (12) degenerates into (7), when the matching range of each node shrinks to only cover itself, the proof readily guarantees the existence of an equilibrium solution for the intranode matching system. The equilibrium solution is likely nonunique for the system considered. Even for an ideal isotropic market without traffic congestion, it has been proved that multiple market equilibria can exist (*Internode matching* Zha, Yin, and Xu 2018).

4.4. Solution Procedure

An iterative algorithm in the same vein as the one proposed by Yang and Wong (1998) is developed to solve the network equilibrium system (12a)–(12x). Before presenting the solution procedure, we first reformulate some conditions into mathematical problems that can easily be solved through commercial solvers.

Specifically, given $\{\boldsymbol{T}^{rs}\}$, Equations (12a)–(12f) can be equivalently reformulated as a convex program PE:

$$\text{(PE)}\quad \min_{\boldsymbol{x},\boldsymbol{v}} \sum_{(i,j)\in A}\int_0^{v_{ij}} t_{ij}(\varpi)\,d\varpi$$
$$\text{s.t.}\quad (12c)-(12f).$$

Furthermore, treating $\{\boldsymbol{T}^{m},\boldsymbol{T}^{o},\boldsymbol{h}\}$ as exogenous variables, the idle RV movements (12k)–(12q) can be captured by using the following mathematical program IRVM:

$$\text{(IRVM)}\ \min_{\boldsymbol{T}^v}\sum_{s\in S}\sum_{l\in L}\left[\left(-\hat{F}_l+\gamma(\hat{h}_l+h_{sl})\right)T_{sl}^v+\frac{1}{\theta}T_{sl}^v(\ln T_{sl}^v-1)\right]$$

$$\text{s.t.}\ \sum_{s\in S}T_{sl}^v=\sum_{r\in M^v(l)}T_{lr}^m \qquad \forall\, l\in L \qquad (13a)$$

$$\sum_{l\in L}T_{sl}^v=\sum_{r:(r,s)\in W}T_{rs}^o \qquad \forall\, s\in S. \qquad (13b)$$

To verify, we examine the Karush–Kuhn–Tucker conditions of IRVM as follows:

$$-\hat{F}_l+\gamma(\hat{h}_l+h_{sl})+\frac{1}{\theta}\ln T_{sl}^v+\beta_l+\tau_s=0 \qquad (13a-b)$$
$$\forall\, l\in L, s\in S, \qquad (14)$$

where $\boldsymbol{\beta}$ and $\boldsymbol{\tau}$ are Lagrangian multipliers associated with (13a) and (13b). From (14), we have

$$-\hat{F}_l+\gamma(\hat{h}_l+h_{sl})+\frac{1}{\theta}\ln T_{sl}^v+\beta_l$$
$$=-\hat{F}_k+\gamma(\hat{h}_k+h_{sk})+\frac{1}{\theta}\ln T_{sk}^v+\beta_k,$$

which is equivalent to

$$\frac{T_{sl}^v}{T_{sk}^v}=\frac{\exp\left\{\theta\left[\hat{F}_l-\gamma\left(\hat{h}_l+h_{sl}+\frac{\beta_l}{\gamma}\right)\right]\right\}}{\exp\left\{\theta\left[\hat{F}_k-\gamma\left(\hat{h}_k+h_{sk}+\frac{\beta_k}{\gamma}\right)\right]\right\}} \qquad \forall\, l,k\in L, s\in S$$

and further yields

$$\frac{T_{sl}^v}{\sum_{r:(r,s)\in W}T_{rs}^o}=\frac{\exp\left\{\theta\left[\hat{F}_l-\gamma\left(\hat{h}_l+h_{sl}+\frac{\beta_l}{\gamma}\right)\right]\right\}}{\sum_{k\in L}\exp\left\{\theta\left[\hat{F}_k-\gamma\left(\hat{h}_k+h_{sk}+\frac{\beta_k}{\gamma}\right)\right]\right\}}$$
$$\forall\, l\in L, s\in S.$$

From this formula, we can interpret the term β_l/γ as the RVs' waiting time at node l (i.e., $w_l^v=\beta_l/\gamma$ for all $l\in L$). As $\boldsymbol{\beta}/\gamma$ is not unique, we can always add a constant η to $\boldsymbol{\beta}/\gamma$, such that the equation still holds.

As per (12x), we have

$$\sum_{(r,s)\in W^c}(T_{rs}^v+T_{rs}^m+T_{rs}^o)\cdot h_{rs}+\sum_{(s,l):s\in S,\,l\in L}\left(\frac{\beta_l}{\gamma}+\eta\right)\cdot T_{sl}^v=N,$$

which gives rise to

$$\eta=\frac{N-\sum_{(r,s)\in W^c}(T_{rs}^v+T_{rs}^m+T_{rs}^o)\cdot h_{rs}-\sum_{(s,l):s\in S,\,l\in L}T_{sl}^v\cdot\beta_l/\gamma}{\sum_{(s,l):s\in S,\,l\in L}T_{sl}^v}$$

and accordingly,

$$w_l^v=\frac{\beta_l}{\gamma}+\eta.$$

We caution that the steps cannot guarantee the nonnegativity of $\boldsymbol{w}^v$. Additional treatment is thus taken in the solution procedure (step 4) to ensure the feasibility of equilibrium produced.

Given the deductions, we develop the following solution procedure to solve the system (12) (see Figure 6 for the corresponding flowchart).

1. Initialize $\boldsymbol{N}^c$, $\boldsymbol{N}^v$, and $\boldsymbol{h}$.
2. Obtain $\hat{\boldsymbol{T}}^m$ by solving (12r)–(12t).
3. Deduce $\tilde{\boldsymbol{w}}^c$ by solving the following equation on each source node $r\in R$:

$$\sum_{s:(r,s)\in W}f_{rs}\left(\beta^o\tilde{w}_r^c+\beta^m\check{h}_r+(\beta^i+\beta^f)h_{rs}\right)=\sum_{l\in M^c(r)}\hat{T}_{lr}^m \qquad \forall\, r\in R.$$

Then, retrieve $\{\hat{\boldsymbol{T}}^o,\hat{\boldsymbol{w}}^c,\hat{\boldsymbol{N}}^c\}$ by letting $\hat{T}_{rs}^o=f_{rs}\left(\beta^o\tilde{w}_r^c+\beta^m\check{h}_r+(\beta^i+\beta^f)h_{rs}\right)$ for all $(r,s)\in W$ and $\hat{w}_r^c=\max\{0,\tilde{w}_r^c\}$, $\hat{N}_r^c=\hat{w}_r^c\cdot\sum_{s:(r,s)\in W}\hat{T}_{rs}^o$ for all $r\in R$.

Figure 6. Solution Procedures

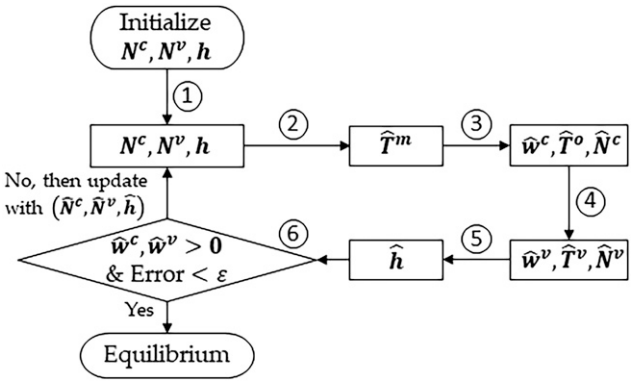

4. Obtain $\{\hat{T}^v, \hat{w}^v\}$ by solving IRVM; then, update $\hat{w}_l^v = \max\{0, \hat{w}_l^v\}$ and $\hat{N}_l^v = \min\{N, \hat{w}_l^v \cdot \sum_{s \in S} \hat{T}_{sl}^v\}$ for all $l \in L$.

5. Obtain $\{\hat{x}, \hat{h}\}$ by solving PE.

6. If $\hat{w}^c, \hat{w}^v > 0$, and $\kappa_c(N^c - \hat{N}^c) + \kappa_v(N^v - \hat{N}^v) + \kappa_h(h - \hat{h}) < \varepsilon$, stop, and the obtained $\{\hat{T}^m, \hat{T}^o, \hat{w}^c, \hat{T}^v, \hat{w}^v, \hat{N}^v, \hat{N}^c, \hat{x}, \hat{h}\}$ is the equilibrium solution; otherwise, update (N^c, N^v, h) using its linear combination with $(\hat{N}^c, \hat{N}^v, \hat{h})$ and repeat the process.

The parameter $\boldsymbol{\kappa}$ in the last step characterizes a set of weights, and ε is a given tolerance. Note that the proof of equilibrium existence in Online Appendix B rationalizes the procedure design. Basically, the system of Equations (12) is transformed into a self-mapping on the set of variables $\{N^c, N^v, h\}$. Deriving the system equilibrium then becomes the problem of finding a fixed-point solution, where the procedure terminates when the conditions before and after the mapping become sufficiently close. The convergence properties of the procedure are not yet theoretically investigated. However, for our extensive numerical experiments in Section 5.2, we have always been successful in achieving convergence on the large-scale Friedrichshain network.

5. Numerical Experiments

This section presents numerical experiments with two networks of different scale. We first use a small-scale Nguyen–Dupius network to illustrate the necessity of considering the internode matching. We show that the intranode model may otherwise yield significant biases in evaluating the vacancy/empty miles generated by RVs of an e-hailing system. We further investigate how RVs' vacancy can be impacted by different market structures on supply and demand. The second set of experiments is conducted on the Friedrichshain (Berlin) network to showcase how the network and market conditions react to various scales of trip demand and RV fleet supply.

Figure 7. (Color online) The Nguyen–Dupius Network

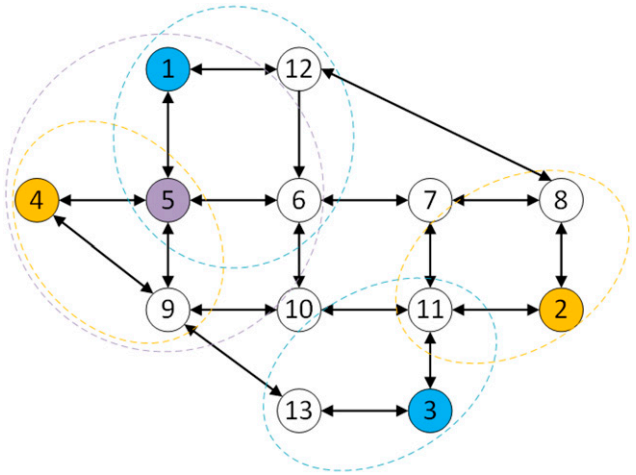

Notes. Origin/destination nodes are highlighted by the filled color. The matching set of each origin node under intranode matching includes itself, whereas the internode counterpart covers the nodes in the circle consistently colored as the origin.

5.1. Experiments on the Nguyen–Dupius Network

The Nguyen–Dupius network (Nguyen and Dupuis 1984) consists of 13 nodes, 38 links, and six OD pairs (see Figure 7). The link performance function is assumed to be a linear one as follows:

$$t_{ij}(v_{ij}) = a_{ij} + b_{ij} \cdot v_{ij} \qquad \forall\ (i,j) \in A.$$

The parameters $\{a_{ij}\}$ and $\{b_{ij}\}$ as well as the regular background vehicular OD demand $\{T_{rs}^n\}$ for the network are provided in Table 3, (a) and (b), respectively, in Online Appendix C.

Let there be ride-sourcing demands between the two node sets {1, 4, 5} and {2, 3} located in the corners of the network (see the filled nodes in Figure 7), and then, specify the customer demand function as

$$f_{rs}(C_{rs}) = Q_{rs}^0 \cdot \exp(-\hat{\theta} C_{rs}) + \epsilon^f / C_{rs} \qquad \forall\ (r,s) \in W,$$

where Q_{rs}^0 in the first term indicates the potential customer demand from node r to s (see Table 3(c) in Online Appendix C). $\hat{\theta}$ features travelers' sensitivity over the cost. ϵ^f in the second term is a small constant. The reciprocal term, which imposes marginal effects under normal conditions, is constructed purposely to ensure the extreme condition $\lim_{w_r^c \to +\infty} w_r^c \cdot f_{rs}(w_r^c | \boldsymbol{h}) \in (0, +\infty)$.

For internode matching, we further specify the potential functions Φ^v, Φ^c and the potential difference function Δ in Equation (12p) as follows:

$$\Phi^v(T_l^v, N_l^v) = (T_l^v)^{-q_T^v} \cdot (N_l^v)^{q_N^v}$$
$$\Phi^c(T_r^c, N_r^c) = (T_r^c)^{-q_T^c} \cdot (N_r^c)^{q_N^c}$$
$$\Delta(T_{lr}^m, h_{lr}) = \eta \cdot T_{lr}^m \cdot (h_{lr})^{q_h},$$

where η, q_h and $\{q_j^i\}_{i \in \{v,c\}, j \in \{T,N\}}$ are parameters. Note

that all parameter values used in the experiments are summarized in Table 3(d) in Online Appendix C for reference.

5.1.1. Necessity of the Internode Matching Model. The matching sets under intranode and internode matching are summarized in Table 3.

Assuming 2,250 RVs in service, equilibrium solutions are then obtained by applying the procedure developed in Section 4.4.

We first compare in Figure 8 the allocations of RVs' service states under the intranode and internode matching. The pie charts show the percentages of RVs that are idle, deadheading, and delivering. Note that in intranode matching, a small, constant intranode pickup time is considered as deadheading whenever a match is made. The RVs' occupancy appears similar in the two cases, whereas the state allocation for vacancy differs drastically. In contrast to the intranode matching counterpart, RVs under internode matching on average experience much less idleness but spend significantly more time on pickup. Such a contrast implies a critical trade-off between waiting (idling) and deadheading of RVs by varying the matching radius, which concerns not only drivers but also, ride-sourcing platforms (see Xu, Yin, and Ye 2020).

Taking the internode equilibrium solution as the baseline, we then compare in detail the differences between these two solutions. Figure 9 displays the relative changes on the link flows as well as RVs and customers' waiting time. The solid and dashed arrows indicate percentage decreases and increases of flows on different links, respectively. The exact percentage difference is provided next to each arrow and shown graphically by its thickness. There is a significantly higher amount of flow on links around the two sets of source nodes under internode matching (e.g., link $5 \rightarrow 4$ and $11 \rightarrow 2$). Further, the columns with upward and downward textures in Figure 9 present the percentage changes on RVs' and customers' waiting times, respectively. Because internode matching enlarges the matching range, thereby reducing the meeting frictions between drivers and customers, both parties' waiting time in matching may decrease compared with the intranode matching counterparts (see, e.g., node 4). Counterexamples, however, arise when the matching sets of two source nodes grow large enough to overlap with each other: for example, the pair of nodes 1 and 5, where node 1 exhibits more significant excess of supply compared with node 5. As a consequence, as we enlarge the matching range to have nodes 1 and 5 overlap substantially in their matching sets, the supply excess condition on the two nodes neutralizes, which yields significantly shorter waiting time for customers on node 5 and RVs on node 1.

Table 3. Matching Sets Under Intranode and Internode Matching

Matching range	$M^c(1)$	$M^c(4)$	$M^c(5)$	$M^c(2)$	$M^c(3)$
Intranode	{1}	{4}	{5}	{2}	{3}
Internode	{1,5,6,12}	{4, 5, 9}	{1,4,5,6,9}	{2, 8, 11}	{3, 11, 13}

The differences suggest that for e-hailing systems with large matching radius, an intranode matching model may drastically bias the estimates of market and network conditions because of the lack of capability of modeling vehicles' deadheading.

5.1.2. Impacts of Market Attributes on RVs' Vacancy. Next, we investigate the impacts of different market attributes on RVs' vacancy. Specifically, this subsection focuses on two system attributes: the level of RVs' fleet supply and the spatial symmetry of customers' demand pattern. The contrasts in supply level are constructed using two fleet sizes, 2,250 and 1,750, which correspond to the condition of sufficiency and shortage, respectively. In addition, we adjust the potential demand portions between the two clusters of origins (1, 4, 5) and (2, 3) (see Figure 7 for specific locations) to differentiate the symmetry of demand patterns. The nominal example introduced characterizes a symmetric case with relatively balanced ride-hailing demand between these two clusters, whereas an asymmetric instance is newly generated by intensifying the demand imbalance (see Table 3(c) in Online Appendix C for the specific setting).

Figure 10 summarizes the allocations of RVs' service states under the four combinations of supply-demand attributes. We obtain the following observation via comparison. In all cases, RVs dedicate around half of their service time to delivery and spend the other half on cruising or deadheading, producing the so-call empty miles. More specifically, compared with the sufficient supply scenario, RVs experience less idleness and higher occupancy under supply shortage. The contrasts appear more noticeable under symmetric demand patterns (see Figure 10(a) versus Figure 10(c) and Figure 10(b) versus Figure 10(d)). Symmetric demand patterns allow idle RVs to get a match quicker after dropping a passenger, yielding a higher occupancy rate. Indeed, demand symmetry increases vehicular occupancy in both insufficient and sufficient supply cases.

5.2. Experiments on the Friedrichshain Network

The small-scale Nguyen–Dupius network example has demonstrated the need for constructing the internode matching model and the capability of the model on capturing ride-sourcing market conditions. In this

Figure 8. (Color online) Allocation of RVs' Service States Under Intra- and Internode Matching

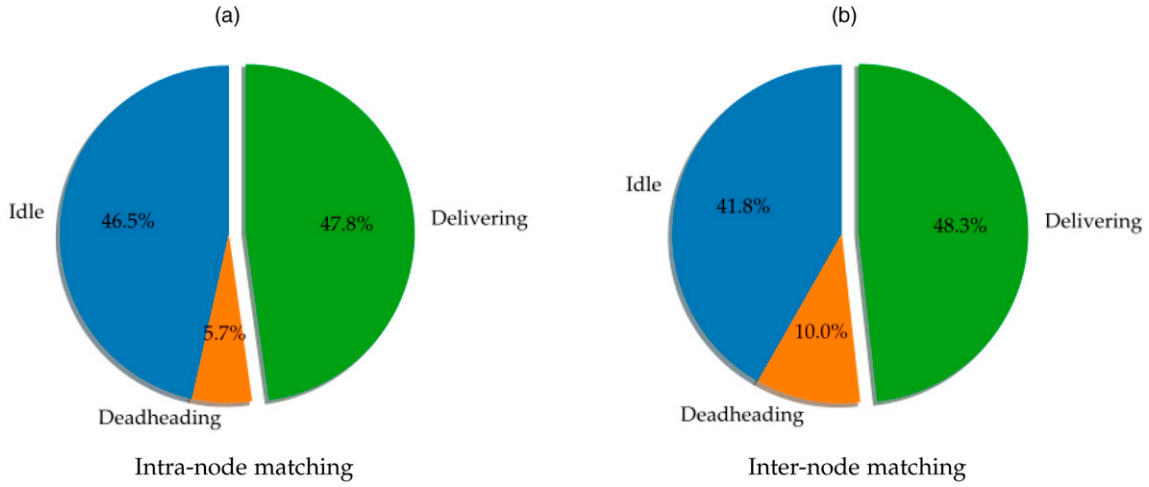

Notes. (a) Intranode matching. (b) Internode matching.

section, we present a second set of experiments with a network based on Friedrichshain, Berlin (see Figure 11 for an overview) to demonstrate how the model can be applied to a realistic network to estimate the network and market conditions. The Friedrichshain network contains 224 nodes, 523 links, and 506 OD pairs. Because of the space limitation, other network data are omitted in this paper, but they are available from the authors upon request.

Our experiments mainly involve two variables: the demand for ride-sourcing services and the total RV supply. We combine these two variables to generate 100 instances to see how the model predicts the network and market conditions. For all these numerical examples,

Figure 9. (Color online) Comparisons of Flow Distributions and Customers and RVs' Waiting Time Under Intra- and Internode Matching

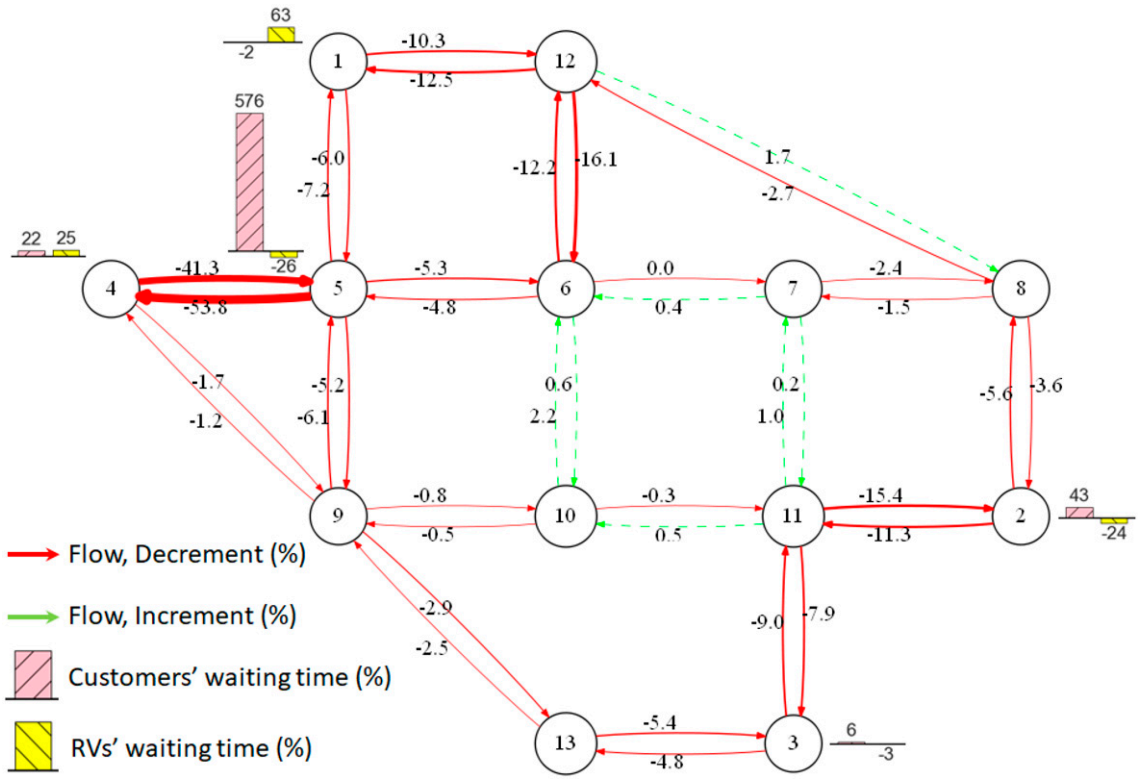

Figure 10. (Color online) Allocations of RVs' Service States Under Different Supply-Demand Contexts

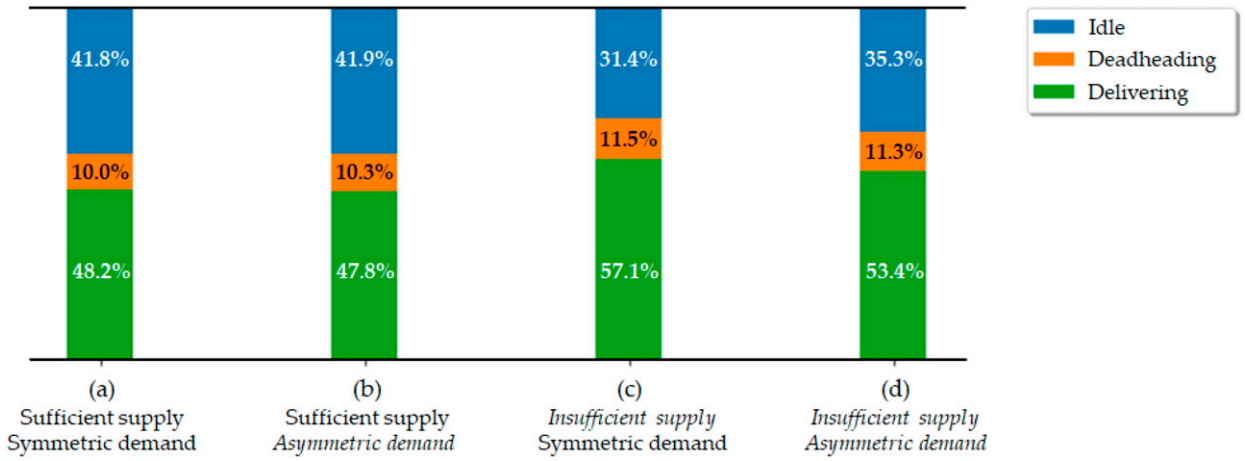

Notes. (a) Sufficient supply and symmetric demand. (b) Sufficient supply and asymmetric demand. (c) Insufficient supply and symmetric demand. (d) Insufficient supply and asymmetric demand.

we have successfully achieved convergence when applying the proposed procedure. The convergence is typically reached within several hundreds of iterations. Each iteration takes about 10 seconds to execute in our GAMS code on a desktop with a 3.30-GHz Intel i5-6600 Processor and 8-GB memory. Two measures are of particular interest: average network running speed to represent the congestion level and the percentage of time being vacant to reflect the ride-sourcing market. Denote Q^0 as the base level of customer demand for ride-sourcing services. We then multiply Q^0 by a demand index α to yield different levels of trip requests.

Figure 11. (Color online) The Friedrichshain Network Containing 224 Nodes and 523 Links

Figure 12. (Color online) Summary of the Ride-Sourcing System's State Statistics

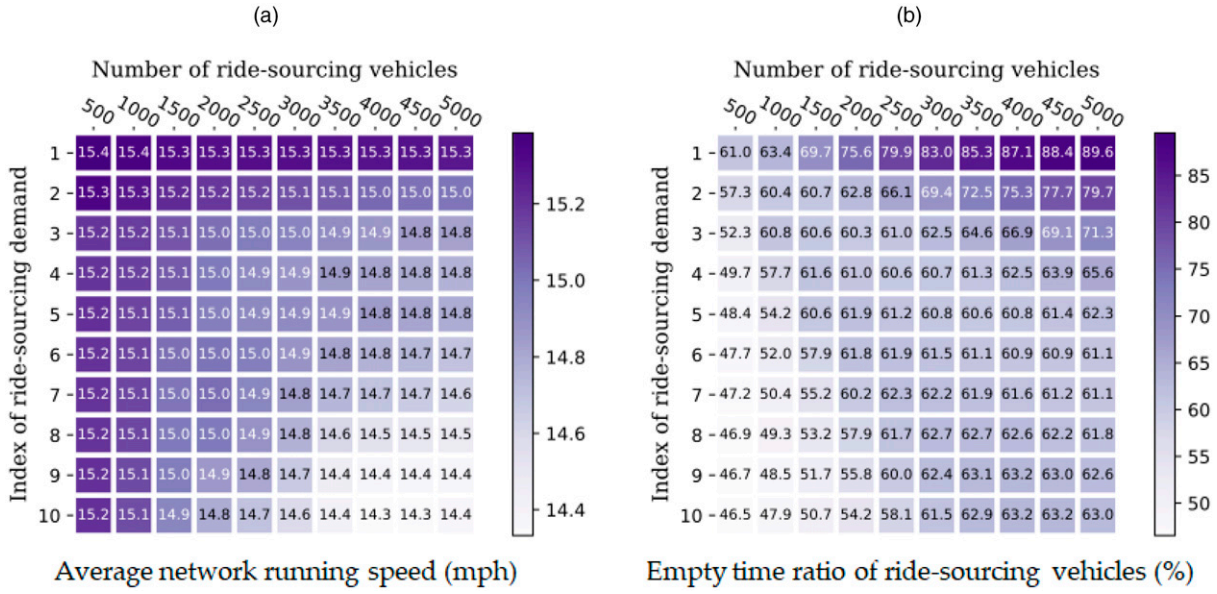

Notes. (a) Average network running speed (miles per hour). (b) Empty time ratio of ride-sourcing vehicles (percentage).

Ten scenarios are considered by varying α from 1 to 10. Additionally, for each level of α, we consider 10 different RV fleet sizes N to replicate different levels of labor supply. Figure 12 summarizes the average network running speed and the average empty time ratio of RVs of these 100 instances.

The average network running speed in Figure 12(a) is calculated as the miles traveled by all the vehicles over the total time they spend on road. As seen from the graph, more demand or supply generally increases congestion. However, when the level of demand (supply) is high, the marginal contribution of additional supply (demand) to congestion is more significant. Figure 12(b) presents the empty time ratio of RVs, which denotes the percentage of time on average RVs spend in idle or deadheading. Intuitively, we observe that the ratio decreases with the demand level while increasing with the supply level. In contrast to the speed measure, the empty time ratio of RVs shows the greatest sensitivity under the low level of demand and high level of supply.

Note that even with severe supply shortage (the lower left corner of Figure 12(b)), the empty time ratio stays above 40%. By allowing a certain level of empty ratio, the ride-sourcing system can endure fewer frictions and operate more smoothly. Thus, it would be meaningful to investigate the optimal empty ratio that maximizes the social welfare of the whole system.

6. Conclusions

This paper proposes an equilibrium traffic assignment model for urban transportation networks where a large portion of travel demand is served by ride-sourcing services. In such networks, other than the occupied vehicular trips transporting travelers from their origins to destinations, massive traffic is contributed by vacant RV trips that originate from the end of one customer trip to the start of the next. Different from existing models, our model takes into account two major types of vacant trips generated by RVs (i.e., cruising and deadheading). We first present a basic model by considering intranode matching between customers and idle RVs. The model characterizes a straightforward extension from Yang and Wong (1998) and is only capable of capturing the congestion effect of cruising trips. To cope with distant matching, a common practice adopted by ride-sourcing platforms, we extend the basic model to incorporate internode matching. Using an analogy to electricity circuits, we propose internode matching function to handle the spatial interaction between neighboring zones in the matching process. Such a specification, as empirically validated using the real-world data from DiDi, endows us with higher flexibility in representing matching strategies of platforms and depicting the movements of vacant RVs. An iterative solution procedure is proposed to solve for the resulting network equilibrium. The numerical examples on the small-scale Nguyen–Dupius network and the realistic Friedrichshain network demonstrate the feasibility of applying our model to predict the performance of a ride-sourcing system and capture its impact on network traffic conditions.

As one of the first attempts of modeling the congestion effect of ride-sourcing services, this paper begins with a static traffic assignment model, which essentially approximates traffic conditions for a certain

time of day, typically peak hours, for a planning purpose. A dynamic assignment model comes as a pending enhancement that better copes with the transient nature of traffic systems but at the same time, demands much heavier computational efforts and data inputs. It is worth noting that the proposed internode matching function is sufficiently flexible for accommodating various assignment techniques and modeling granularity. As exemplified in the empirical analysis, the function can be easily customized to deal with the time-dependent system variations and offer high-quality predictions. For future research, we plan to develop guidance for transportation planning agencies on specifying the parametric values for the internode matching function. In fact, as we mention in Section 3.3, empirically calibrating the matching function may encounter the endogeneity problem because the specified covariates are deeply connected in a real system. Special model constructions are thus needed to help fully identify the impacts of different market factors. We hope that the proposed modeling framework can help government agencies with their policy making in regulating or managing a ride-sourcing system.

Endnotes

[1] Intranode matching flows in this framework are essentially indicated by $\{T^m_{rr}\}$, $\forall\, r \in R$.

[2] The logarithm associated with the potentials (also the potential differences defined later) seems unnecessary, but it facilitates making a connection with a Cobb–Douglas-type matching function.

[3] Equation 9(a) results from the internal relations among potentials that $\phi^v_l - \phi^c_r = \delta\phi_{lr}$. The effectiveness of such a physical construct is validated empirically in Section 3.3.

[4] Big Θ pertains to one of the Bachmann–Landau notations. By writing $f(n) = \Theta(g(n))$, it means f is asymptotically bounded both above and below by g.

[5] Note that hexagonal partitioning is utilized in this empirical analysis of internode matching, taking advantage of the ride-sourcing platform's existing treatments. However, in the cases of network equilibrium analysis, which involves traffic congestion, a zoning system compatible with census blocks and road geometries needs to be adopted.

[6] Quantitatively, an effective zonal pair is determined as the one having more than 300 passenger-driver matches throughout the year of 2019.

[7] We suggest readers review Section 4.4 before reading the proof in the online appendix, as some mapping systems defined in the former are referred in the proof.

References

Anderson M (2019) Mobile technology and home broadband 2019. Pew Research Center (June 13), https://www.pewresearch.org/internet/2019/06/13/mobile-technology-and-home-broadband-2019/.

Ban XJ, Dessouky M, Pang J-S, Fan R (2019) A general equilibrium model for transportation systems with e-hailing services and flow congestion. *Transportation Res. Part B: Methodological* 129:273–304.

Castiglione J, Cooper D, Sana B, Tischler D, Chang T, Erhardt GD, Roy S, Chen M, Mucci A (2018) TNCs & congestion. Technical report, San Francisco County Transportation Authority, San Francisco.

Castillo JC, Knoepfle DT, Weyl EG (2016) Matching in ride hailing: Wild Goose chases and how to solve them. Preprint, submitted December 28, http://dx.doi.org/10.2139/ssrn.2890666.

Douglas GW (1972) Price regulation and optimal service standards: The taxicab industry. *J. Transport Econom. Policy* 6(2):116–127.

Erhardt GD, Roy S, Cooper D, Sana B, Chen M, Castiglione J (2019) Do transportation network companies decrease or increase congestion? *Sci. Adv.* 5(5):eaau2670.

Greer L, Fraser JL, Hicks D, Mercer M, Thompson K (2018) Intelligent transportation systems benefits, costs, and lessons learned: 2018 update report. Technical Report No. FHWA-JPO-18-641, U.S. Department of Transportation ITS Joint Program Office, Washington, DC.

Hall MA (1978) Properties of the equilibrium state in transportation networks. *Transportation Sci.* 12(3):208–216.

He F, Shen ZJM (2015) Modeling taxi services with smartphone-based e-hailing applications. *Transportation Res. Part C: Emerging Tech.* 58:93–106.

Iqbal M (2019) Uber revenue and usage statistics. *Business of Apps*. Accessed June 20, 2019, http://www.businessofapps.com/data/uber-statistics/.

Nguyen S, Dupuis C (1984) An efficient method for computing traffic equilibria in networks with asymmetric transportation costs. *Transportation Sci.* 18(2):185–202.

Qu X, Wang S, Zhang J (2015) On the fundamental diagram for freeway traffic: A novel calibration approach for single-regime models. *Transportation Res. Part B: Methodological* 73:91–102.

Schaller B (2018) The new automobility: Lyft, Uber and the future of American cities. Technical report, Schaller Consulting, Brooklyn, NY.

Wong KI, Wong SC, Yang H (2001) Modeling urban taxi services in congested road networks with elastic demand. *Transportation Res. Part B: Methodological* 35(9):819–842.

Wong KI, Wong SC, Yang H, Wu JH (2008) Modeling urban taxi services with multiple user classes and vehicle modes. *Transportation Res. Part B: Methodological* 42(10):985–1007.

Xu Z, Yin Y, Ye J (2020) On the supply curve of ride-hailing systems. *Transportation Res. Part B: Methodological* 132:29–43.

Yang H, Wong SC (1998) A network model of urban taxi services. *Transportation Res. Part B: Methodological* 32(4):235–246.

Yang H, Yang T (2011) Equilibrium properties of taxi markets with search frictions. *Transportation Res. Part B: Methodological* 45(4): 696–713.

Yang H, Wong SC, Wong KI (2002) Demand-supply equilibrium of taxi services in a network under competition and regulation. *Transportation Res. Part B: Methodological* 36(9):799–819.

Yang H, Leung CW, Wong SC, Bell MG (2010) Equilibria of bilateral taxi-customer searching and meeting on networks. *Transportation Res. Part B: Methodological* 44(8): 1067–1083.

Zha L, Yin Y, Xu Z (2018) Geometric matching and spatial pricing in ride-sourcing markets. *Transportation Res. Part C: Emerging Tech.* 92:58–75.

Zha L, Yin Y, Yang H (2016) Economic analysis of ride-sourcing markets. *Transportation Res. Part C: Emerging Tech.* 71:249–266.